Isoform-specific roles of the *Drosophila* filamin-type protein Jitterbug (Jbug) during development

SeYeon Chung[1, ¶, *], Thao Phuong Le[1, ¶], Vishakha Vishwakarma[1], Yim Ling Cheng[2] and Deborah J. Andrew[2]

[1] Department of Biological Sciences, Louisiana State University, Baton Rouge, LA 70803, USA

[2] Department of Cell Biology, Johns Hopkins University School of Medicine, Baltimore, MD 21205, USA

¶ These authors contributed equally to this work.

[*]Author for correspondence: seyeonchung@lsu.edu

Running title: Roles of Jitterbug in *Drosophila* development

Key workds: *Drosophila*, filamin, *jitterbug*, actin, thoracic bristles, epidermal denticles, tubular epithelial organs, trans-splicing, Crb

ABSTRACT

Filamins are highly conserved actin-crosslinking proteins that regulate organization of the actin cytoskeleton. As key components of versatile signaling scaffolds, filamins are implicated in developmental anomalies and cancer. Multiple isoforms of filamins exist, raising the possibility of distinct functions for each isoform during development and in disease. Here, we provide an initial characterization of *jitterbug* (*jbug*), which encodes one of the two filamin-type proteins in *Drosophila*. We generate Jbug antiserum that recognizes all of the spliced forms and reveals differential expression of different Jbug isoforms during development, and a significant maternal contribution of Jbug protein. To reveal the function of Jbug isoforms, we create new genetic tools, including a null allele that deletes all isoforms, hypomorphic alleles that affect only a subset, and UAS lines for Gal4-driven expression of the major isoforms. Using these tools, we demonstrate that Jbug is required for viability and that specific isoforms are required in the formation of actin-rich protrusions including thoracic bristles in adults and ventral denticles in the embryo. We also show that specific isoforms of Jbug show differential localization within epithelia and that maternal and zygotic loss of *jbug* disrupts Crumbs (Crb) localization in several epithelial cell types.

Introduction

Actin-crosslinking proteins organize actin filaments into higher-order structures such as orthogonal actin arrays and parallel actin bundles. Filamins are highly conserved large cytoplasmic proteins that crosslink actin filaments into dynamic three-dimensional structures (Nakamura *et al.* 2011; Razinia *et al.* 2012). Filamins consist of actin-binding Calponin-homology (CH) domains at their N-terminus, followed by a long C-terminal rod-like domain of filamin-type immunoglobulin (IG-FLMN) repeats. Dimerization of filamins through the last C-terminal IG-FLMN repeat allows the formation of a flexible V-shaped structure that holds two actin filaments at large angles to create either a loose three-dimensional actin network (Nakamura *et al.* 2011; Razinia *et al.* 2012) or parallel bundles of actin filaments (Sokol and Cooley 1999; Gay *et al.* 2011). In addition to binding to actin, filamins interact with transmembrane receptors, adhesion molecules and even transcription factors, and are thus involved in multiple cell functions, including motility, maintenance of cell shape, and differentiation (Nakamura *et al.* 2011; Razinia *et al.* 2012). Mutations in filamins are associated with a wide range of congenital anomalies and have been shown to both promote and inhibit metastasis and cancer growth (Razinia *et al.* 2012; Savoy and Ghosh 2013; Shao *et al.* 2016; Sasaki *et al.* 2019), emphasizing the multiple critical roles of filamins in development and disease.

Studies in *Drosophila* have helped refine our understanding of the roles of filamins in vivo. *Drosophila* has two orthologs of human filamin A: Cheerio (Cher) and Jitterbug (Jbug). Cher shares the organization of the protein and 46% identity and 61% similarity in amino acid sequence with human filamin A. Jbug, with 23% identity and 36% similarity in amino acid sequence with human filamin A, has some distinct features, including an actin-binding domain consisting of three, instead of two, CH domains. Several studies have revealed roles for Cher in organizing the F-actin cytoskeleton in multiple developmental contexts and diseases, including formation of ovarian germline ring canals (Li *et al.* 1999; Sokol and Cooley 1999; Huelsmann *et al.* 2016), follicle cell migration (Sokol and Cooley 2003), tissue morphogenesis during cellularization (Krueger *et al.* 2019), and *Drosophila* tumorigenesis (Külshammer and Uhlirova 2013). Compared to the extensive studies on Cher, our understanding of the roles of Jbug is more limited. Originally identified as a gene that causes bang-sensitive seizure – the phenotype that gives the gene its *jitterbug* name (Song and Tanouye 2006), *jbug* is required in photoreceptor cells for axon targeting (Oliva *et al.* 2015) and in tendon cells to maintain their shape at the muscle-tendon junction (Olguín *et al.* 2011; Manieu *et al.* 2018).

71 Multiple isoforms of filamin proteins exist in both *Drosophila* and mammals (Sokol and Cooley
72 1999; Browne *et al.* 2000; Van der Flier and Sonnenberg 2001; Gorlin *et al.* 1990; Wang *et al.*
73 2007). Originally, only two Cher isoforms were reported: a large isoform (FLN240) that contains
74 both actin-binding CH domains and IG-FLMN repeats and a smaller one (FLN90) that contains
75 only IG-FLMN repeats (Sokol and Cooley 1999). Recent annotations indicate that *cher* encodes
76 six longer isoforms (>240 kDa), which include two actin-binding CH domains and 18-22 IG-FLMN
77 repeats, and four shorter isoforms (90-100 kDa), which include only eight IG-FLMN repeats
78 without any CH domains (Flybase; www.flybase.org; Thurmond *et al.* 2019). Importantly, a recent
79 study in *Drosophila* larval neuromuscular junctions revealed a role for the shorter Cher isoform
80 (FLN90) as a postsynaptic scaffold in *Drosophila* larval neuromuscular junctions during synapse
81 formation (Lee and Schwarz 2016), suggesting distinct roles for different isoforms. Like *cher*, *jbug*
82 also encodes multiple isoforms with a range of protein sizes. However, the roles for *jbug* have
83 been revealed mostly using RNA interference (RNAi) constructs that target most of the existing
84 splice forms (Olguín *et al.* 2011; Manieu *et al.* 2018), preventing the characterization of isoform-
85 specific roles for Jbug.

86 Here, we report on the creation of several new genetic tools for parsing out the roles of the
87 different Jbug isoforms, including a null allele that deletes all isoforms and hypomorphic alleles
88 that affect only a few. We also create UAS constructs for expressing the major Jbug isoforms. We
89 demonstrate that different isoforms are differentially expressed during development and localize
90 to different domains in embryonic epithelia. We show isoform-specific roles of Jbug in formation
91 of epidermal denticles during embryogenesis and thoracic bristles in adults. Finally, we also report
92 that removal of both maternal and tissue-specific supplies of *jbug* disrupts tissue morphology and
93 reduces Crb accumulation in the subapical domain of epithelial cells.
94

Materials and Methods

Fly stocks and husbandry

Fly lines used in our experiments were: *Oregon R*; *jbug*^{20}, *jbug*^{30}, *jbug*^{133}, UAS-Jbug-RC, UAS-Jbug-RI, UAS-Jbug-RF (this work); UAS-Jbug-RL (Olguín *et al.* 2011); *fkh-Gal4* (Henderson and Andrew 2000); *69B-Gal4* (Rorth 1996); *da-Gal4* (Wodarz *et al.* 1995); *mat*α*-Gal4* (Häcker and Perrimon 1998), *Df(2R)59AB*, *Df(2R)Exel6079*, *TRiP.JF01166* (Bloomington Stock Center); *GD8664*, *GD13033* (Vienna *Drosophila* RNAi Center). All crosses were performed at 25°C.

Generation of *jbug* mutant alleles

jbug mutants were generated by homologous recombination (Gong and Golic 2003). For *jbug*^{20} null mutants, genomic fragments upstream and downstream of the *jbug* ORF were amplified by PCR using the following primers (restriction sites in bold and linkers in italic):

in-fusion_L-22737893, 5'-*CTAGTCTAGGGCGCGCC*GATGAGTTGTGGCTTGAGCA-3'
in-fusion_R-22742442, 5'-*TAGGGGATCACGTACG*GCCAAACCAATGCTGAAGAT-3'
NotI_L-22717574, 5'-AT**GCGGCCGC**TAGAGGGGAGAGCAAGTGGA-3'
Acc65I_R-22721186, 5'-ATA**GGTACC**GTGTGAGCTTCGGGATCAAT-3'

For *jbug*^{30} and *jbug*^{133} hypomorphic alleles, genomic fragments upstream and downstream of an exon common to all *jbug* splice forms were amplified using the following primers (restriction sites in bold):

AscI_L-22727168, 5'-AT**GGCGCGCC**AAAGCCGTTGAAGAAAGCAA-3'
BsiWI_R-22731840, 5'-ATA**CGTACG**CTCGATGCACTTTGTCTCCA-3'
NotI_L-22717574, 5'-AT**GCGGCCGC**TAGAGGGGAGAGCAAGTGGA-3'
Acc65I_R-22721186, 5'-ATA**GGTACC**GTGTGAGCTTCGGGATCAAT-3'

PCR fragments were cloned into pW25, which carries *white*$^{+}$, the recognition site for I-SceI endonuclease, and FRT sites. The constructs were injected into *w*^{1118} embryos by Rainbow Transgenic Flies, Inc. Transformants were crossed to flies carrying hs-I-SceI and hs-Flp, and progeny were heat shocked (37°C) for 1 hour 48–72 hours after egg laying (AEL). Recombination and insertion were confirmed by genomic PCR and reverse-transcriptase PCR (RT-PCR) followed by sequencing.

125 The following primers were used for RT-PCR for *jbug*[20] shown in Supplemental Figure 2
126 (restriction sites in bold and linkers in italic):

127 *jbug* 5-1, 5'-GGAGAACAAGTACCGGGTGA-3'
128 *jbug* 5-2, 5'-*GGATCCTCGAGCATATG*TCCTTCCACGTTCACCTCGA-3' (same as Jbug-Ab-3' for
129 making Jbug antibody)
130 *jbug* 3-1, 5'-AT**GCGGCCGC**TAGAGGGGAGAGCAAGTGGA-3' (same as NotI_L-22717574 used
131 for amplifying a homology arm downstream of the *jbug* ORF)
132 *jbug* 3-2, 5'-*CGCGCGGCAGCCATATG*ATGTCCTCACCCGGCCTAAC-3' (same as Jbug-Ab-5'
133 for making Jbug antibody)
134

135 **Generation of UAS-Jbug-RC, -RI and -RF transgenic flies**

136 An ORF for *jbug-RC* (1230 bp) was PCR-amplified using the existing cDNA RE40504 as a
137 template. A full length cDNA for *jbug-RF* (9430 bp) was created by In-Fusion cloning of three
138 fragments. The 5' fragment was prepared by enzyme digestion of RE40504 (cut with ApaI and
139 BamHI). The middle fragment (1189 bp) was amplified by reverse transcriptase-PCR (RT-PCR),
140 and the ApaI and BglII sites were added to the 5' and the 3' end of the fragment, respectively.
141 The 3' fragment was amplified by PCR using the existing cDNA GH03118 from the BglII site to
142 the end of the ORF, and the BamHI site was added to the 3' end. The ligated full cDNA was
143 confirmed by sequencing. A full cDNA for *jbug-RI* (5989 bp) was created by PCR amplification
144 using the *jbug-RF* cDNA as a template and confirmed by sequencing. *jbug-RC*, *jbug-RI* and *jbug-*
145 *RF* ORFs were PCR-amplified and cloned into the pUAST vector (Brand and Perrimon, 1993) to
146 create UAS lines. The DNA constructs were injected into w^{1118} embryos by Rainbow Transgenics,
147 Inc. (UAS-Jbug-RC) and GenetiVision (UAS-Jbug-RI and UAS-Jbug-RF).
148

149 **Generation of Jbug antibody**

150 A PCR fragment of 1212 bp common to all *jbug* splice forms was cloned into the pET15b vector.
151 The fragment corresponds to almost the entire open reading frame for the Jbug-PC isoform
152 except for the last six amino acids and contains four IG-FLMN repeats. Primers used for In-Fusion
153 cloning were (linkers in italic):

154 Jbug-Ab-5', 5'- *CGCGCGGCAGCCATATG*ATGTCCTCACCCGGCCTAAC-3'
155 Jbug-Ab-3', 5'- *GGATCCTCGAGCATATG*TCCTTCCACGTTCACCTCGA-3'

156 The construct was transformed into BL21-DE3 cells for protein induction with IPTG. Recombinant
157 protein was purified using Ni-NTA agarose (Qiagen). Rabbit polyclonal antibodies were generated
158 by Covance, Inc. and used at a dilution of 1:500 for immunohistochemistry and 1:5,000 for western
159 blot.
160
161 **Whole-mount in situ hybridization**
162 In situ hybridization was performed as described previously (Lehmann and Tautz 1994). Probes
163 specific for a subset of *jbug* splice forms are shown in Figure 1A. DNA fragments for probes 1
164 and 3 were PCR-amplified using wild-type genomic DNA, cloned into the pCR2.1 vector and
165 sequenced to verify. Probe 2 was made from cDNA GH03013, linearized at the KpnI site to create
166 a probe specific to all jbug splice forms. Antisense digoxigenin-labeled RNA probes were
167 generated using T7 (probes 1 and 3) or SP6 (probe 2) polymerase on linearized templates. The
168 molecular regions corresponding to the RNA probes are as follows:

169 Probe 1 (specific for *jbug-RF/M/N* and *jbug-RL*): 22734199 – 22731666
170 Probe 2 (detects all *jbug* transcripts): 22722586-22722906, 22723936-22724162, 22724531-
171 22725474
172 Probe 3 (specific for *jbug-RF/M/N* and *jbug-RI*): 22721775 – 22720075
173
174 **Western blot**
175 Protein extracts from embryos 0-2 and 2-16 hours AEL, 1st, 2nd, 3rd instar larvae, pupae (2 days
176 after puparium formation (APF), and 2-day old male and female adults were used. For embryos
177 homozygous for *jbug*^{20}, *Df(2R)59AB* and *Df(2R)Exel6079* and for 1st instar larvae homozygous
178 for *jbug*^{20} and transheterozygous for *jbug*^{30}/*Df(2R)Exel6079*, a balancer chromosome that
179 contains the twi-Gal4 UAS-GFP construct was used to distinguish desired genotypes from
180 heterozygous siblings. Rabbit α-Jbug (this work; 1:5,000), mouse α-Actin (RRID:AB_11004139;
181 Invitrogen; 1:2,000), and HRP-labelled secondary antibodies (RRID:AB_430833;
182 RRID:AB_430834; Promega; 1:2,000) were used. Protein bands were detected using Pierce ECL
183 Western Blotting Substrate.
184
185 **Scanning electron microscopy**
186 Wild type (*Oregon R*) and *jbug*^{30} homozygous male flies were coated with gold palladium and
187 examined and photographed in a LEO/Zeiss Field-emission SEM.
188

189 **Antibody staining and confocal microscopy**

190 Embryos were collected on grape juice-agar plates and processed for immunofluorescence using
191 standard procedures. Briefly, embryos were dechorionated in 50% bleach, fixed in 1:1
192 heptane:formaldehyde for 40 min and devitellinized with 80% EtOH, then stained with primary
193 and secondary antibodies in PBSTB (1X PBS, 0.1% Triton X-100, 0.2% BSA). For Jbug and
194 phalloidin staining, embryos were hand-devitellinized. Antibodies used include: mouse α-Crb
195 (RRID:AB_528181; DSHB (Cq4); 1:10), mouse α-α-Spec (RRID:AB_528473; DSHB (3A9); 1:2) ,
196 rabbit α-Neurexin IV (Baumgartner *et al.* 1996; 1:2,000), rabbit α-CrebA (RRID:AB_10805295;
197 1:5,000), guinea pig α-Sage (Fox *et al.* 2013; 1:100), chicken α-GFP (RRID:AB_2534023;
198 Invitrogen; 1:500), rat α-E-Cad (RRID:AB_528120; DSHB (DCAD2); 1:50), rabbit α-Jbug (this
199 work; 1:500), rabbit α-β-Gal (RRID:AB_221539; Invitrogen; 1:500). Alexa fluor 488, 568, 647-
200 labelled secondary antibodies were used at 1:500 (RRID:AB_142924; RRID:AB_141778;
201 RRID:AB_2535766; RRID:AB_143157; RRID:AB_2535812; Molecular Probes). Alexa fluor-568-
202 labeled phalloidin was used for F-actin labelling (RRID:AB_2632953; Molecular Probes; 1:250).
203 All images were taken with a Leica SP8 confocal microscope using either a 63x, 1.4 NA or a 40x,
204 1.3 NA oil objective and the LAS X software (Leica).

205

206 **Quantification of denticle precursors in the ventral epidermis**

207 Embryos stained for phalloidin and E-Cad were imaged with a Leica SP8 confocal microscope. A
208 maximum intensity projection was generated using two focal planes (0.3 μm apart) in the region
209 of adherens junctions. Denticle belts in abdominal segments 4-6 in stage 16 embryos were
210 selected for quantification. Six columns of cells from anterior to posterior of each belt were
211 analyzed. In each column, denticle precursors of four cells closest to the ventral midline were
212 counted. For each genotype, five to eight embryos were quantified. Unpaired Student's t-test with
213 Welch's correction was used for statistical analysis.

214

215 **Data availability**

216 All data and methods required to confirm the conclusions of this work are within the article, figures,
217 and supplemental materials.

Results

Different splice forms of *jbug* are differentially expressed during development

Ten annotated splice forms of *jbug*, which encode six different protein isoforms, are reported in Flybase (www.flybase.org; Thurmond *et al.* 2019). All isoforms contain multiple repeats of filamin-type immunoglobulin (IG-FMLN) domains (Figure 1, A and B), which form a rod-like structure in filamin. Two Jbug isoforms consist exclusively of these repeats; Jbug-PC/G/H/J/K (each splice form encodes the same 42.4 kDa protein; hereafter referred to as Jbug-PC) has four IG-FMLN repeats and Jbug-PI (185.7 kDa) has sixteen (Figure 1B). On the other hand, Jbug-PL (175.6 kDa) and Jbug-PF/M/N, the three longest Jbug isoforms (>300 kDa), contain three tandem calponin-homology (CH) actin-binding domains in their N-termini as well as multiple IG-FMNLs in their C-termini (seven and nineteen IG-FMLNs for Jbug-PL and Jbug-PF/M/N, respectively) (Figure 1B).

High-throughput expression data available in Flybase (www.flybase.org; Thurmond *et al.* 2019) showed high expression of *jbug* splice forms throughout all developmental stages, except during 0-10 hours of embryogenesis when there is a minimal expression of *jbug-RF/M/N* and *jbug-RL* (Figure 1C). BDGP Expression Data showed that, in addition to the strong ectodermal expression at earlier stages, *jbug* is also upregulated in epithelial tubular organs, including the trachea primordia and the salivary gland (https://insitu.fruitfly.org/cgi-bin/ex/insitu.pl). Our previous work confirmed this expression and revealed that *jbug* tracheal expression requires Trachealess, a major transcription factor in the trachea (Chung *et al.* 2011).

in situ hybridization using probes specific for different *jbug* splice forms further revealed tissue-specific expression of specific *jbug* splice forms (Supplemental Figure 1). A 5' probe (Figure 1A; probe1) that should detect *jbug-RL* (the form that includes the CH actin-binding domains) and the longest splice forms *jbug-RF/M/N* revealed no expression until embryonic stage 12, when expression in the clypeolabrum (CL) was first detected at low levels (Supplemental Figure 1, left column). This CL expression persisted through embryogenesis with later additional expression in another group of anterior cells that, together with the CL-positive cells, forms the mouth and low level expression in posterior cells that form the posterior spiracles. A 3' probe (Figure 1A; probe 3) that detects *jbug-RI* (the form that includes sixteen IG-FLMN repeats without the CH actin-binding domains) and *jbug-RF/M/N* reveals broad ectodermal expression in early embryos, with tissue-specific expression apparent by stage 11 in the CL, salivary gland, and tracheal pits (tp), with some low level expression in the foregut and subset of midline cells (Supplemental Figure 1; right column). By stage 12, the CL and tp staining are no longer detectable and expression is now also observed in epidermal stripes. By late stages, expression is also observed in the region of

251 the posterior spiracles. A probe that detects all *jbug* splice forms (Figure 1A, probe 2) revealed a
252 pattern that was the sum of the expression patterns observed with the more 5' and 3' isoform-
253 specific probes. Given the very limited overlap in staining patterns with the 5' (probe 1) and 3'
254 (probe 3) probes, this finding suggests that *jbug-RL* and *jbug-RI* are the major mRNA splice forms
255 made in embryos and that *jbug-RL* is much more restricted in its expression than *jbug-RI*, both in
256 terms of how early the transcripts are detected and how broadly expression is observed. If *jbug*
257 *RF/M/N* transcripts are produced in embryos, the expression must be limited to the late posterior
258 spiracles, the only site where all three probes detected signals. Likewise, if *jbug-RC* is made in
259 embryos, it must completely overlap the expression patterns of *jbug-RL* and *jbug-RI*.

260 To analyze protein expression levels of Jbug during *Drosophila* development, we generated Jbug
261 antiserum that recognizes a protein domain encoded by all ten *jbug* splice forms (Figure 1A). This
262 domain includes the four IG-FLMN repeats present in all Jbug isoforms (Figure 1B). Our Western
263 blot analysis using wild-type protein extracts revealed that Jbug proteins are detected at high
264 levels throughout all developmental stages (Figure 1D). Strong Jbug signals in protein extracts
265 from 0-2 hour embryos (Figure 1D) also suggest a maternally provided pool of Jbug. The Jbug
266 antiserum detected bands in size ranges predicted from the major splice forms (42.4 kDa, 175.6
267 kDa, 185.7 kDa, >300 kDa). Importantly, the different isoforms were differentially expressed
268 during development (Figure 1D). Jbug-PC (42.4 KDa) was abundant only in pupae and Jbug-PL
269 (175.6 kDa) was most abundant in adults (Figure 1D). Bands corresponding in size to Jbug-PI
270 (185.7 kDa) and Jbug-PF/M/N (>300 kDa) were detected at all stages with slight differences in
271 protein levels. The PI band had the highest intensity at almost all stages, with the exception of
272 PC in pupae, where the levels of PI and PC were similar (Figure 1D). Jbug-PF/M/N isoforms differ
273 only slightly from one another in regions outside the CH and IG-FLMN domains. Due to their huge
274 sizes and a very slight difference in molecular weight among Jbug-PF/M/N, we were not able to
275 distinguish exactly which of the three isoforms is expressed at any specific stage. The large size
276 of these isoforms potentially also diminishes membrane transfer, potentially leading to relatively
277 weak signals. Alternatively, the relatively weak signals could indicate that only very low levels of
278 the longest splice forms are made. Notably, several intermediate-sized bands that did not match
279 the predicted size of annotated isoforms were also detected at different levels throughout
280 development (Figure 1D). The existence of these bands suggests either that more Jbug isoforms
281 exist than have been annotated or that proteolyzed and/or phosphorylated fragments are being
282 detected (also see Figure 1E; most of these extra bands are absent in *jbug* null mutant larval
283 extracts). Indeed, roles for proteolytic forms of Filamin A (Bedolla *et al.* 2009; Savoy and Ghosh

284 2013; Yue *et al.* 2013) as well as phosphorylated Filamin A (Ohta and Hartwig 1996; Tirupula *et*
285 *al.* 2015) have been reported from studies of the mammalian proteins. Overall, our data indicate
286 that different splice forms of *jbug* are differentially expressed during *Drosophila* development.
287

288 **Null and hypomorphic *jbug* alleles have been generated**

289 To investigate roles for *jbug* in development, we generated mutant alleles for *jbug* using
290 homologous recombination (Gong and Golic 2003). Two donor DNA constructs were used to
291 target different genomic regions. One construct targets the genomic region encompassing the
292 translation start sites for all splice forms and extends through the exons shared by all splice forms;
293 the other targets only the region containing the exons shared by all splice forms. With the
294 construct that targets the larger region, we obtained a null mutant, $jbug^{20}$ (Figure 1A). PCR
295 analysis confirmed that the entire targeted region was replaced with the mini-$white^{+}$ (mini-w^{+})
296 gene (data not shown). Reverse transcriptase-PCR (RT-PCR) using mRNA extracted from
297 homozygous $jbug^{20}$ embryos further confirmed that no *jbug* transcripts are produced in $jbug^{20}$
298 embryos (Supplemental Figure 2, A-C). Both $jbug^{20}$ homozygous animals and transheterozygotes
299 for $jbug^{20}$ over either of the two deficiency lines that delete all or part of the *jbug* locus (*59AB* and
300 *Exel6079*; Figure 1A) died during the first instar larval stage (Figure 1H; Table 1). Western blot
301 analysis using Jbug antiserum showed that whereas a significant amount of the Jbug proteins
302 were detected in $jbug^{20}$ embryos (Figure 1, E and H), almost all protein bands were absent by the
303 first instar larval stage, with the exception of two low molecular weight bands that are likely to be
304 from nonspecific cross-reactivity (Figure 1E). Similarly, the same Jbug isoforms were detected
305 both in *59AB* and *Exel6079* homozygous embryos as observed in WT (Figure 1F). These data
306 suggest that Jbug proteins from maternally provided *jbug* mRNA or protein persist through
307 embryogenesis. Since only very low level *jbug* mRNA is detected in 0-2 hour wild-type embryos,
308 based on RNA-Seq (Figure 1C, Flybase; www.flybase.org) and in situ hybridization (Fly-FISH;
309 http://fly-fish.ccbr.utoronto.ca; BDGP; https://insitu.fruitfly.org/cgi-bin/ex/insitu.pl; this study), it is
310 the Jbug protein and not *jbug* mRNA, that is maternally provided.

311 With the DNA construct that aimed to remove the genomic region common for all splice forms of
312 *jbug*, we unexpectedly obtained two hypomorphic alleles, $jbug^{30}$ and $jbug^{133}$, that affect only a
313 subset of splice forms. Incomplete recombination occurred in these two alleles, resulting in either
314 a part of (for $jbug^{30}$) or the entire DNA construct (for $jbug^{133}$) being inserted into the *jbug* locus
315 (Figure 1, A' and A''). In $jbug^{30}$, the more 3' homology arm in the donor DNA recombined correctly,
316 but the other homology arm was inserted into the genome along with the mini-*w*+ gene, rather

317 than being recombined (Figure 1A'). In *jbug*^{133}, homologous recombination failed to occur; instead,
318 the entire donor construct was inserted into the 3' UTR of the splice forms that have longer C-
319 termini (*jbug-RI* and *jbug-RF*/*M*/*N*) (Figure 1A''). These recombination events disrupted *jbug-RI*
320 and *jbug-RF*/*M*/*N* in both alleles. Western blot analysis revealed that the Jbug-PF/M/N isoforms
321 (>300 kDa) were either absent or decreased to undetectable levels in *jbug*^{30} mutants at all stages
322 (Figure 1E). Jbug-PI (185.7 kDa) was also absent in *jbug*^{30}, and instead, a smaller protein (~90
323 kDa) was detected in *jbug*^{30} mutant animals at all stages (Figure 1, E and H). This additional band
324 was not detected in wild-type or *jbug*^{133} protein extracts at any stage, suggesting that insertion of
325 the DNA construct generates a truncated form of Jbug-PI in *jbug*^{30}. In *jbug*^{133}, both Jbug-PF/M/N
326 and Jbug-PI protein bands were slightly decreased in intensity (Figure 1, E and H), suggesting
327 that insertion of the construct in the 3' UTR region either affects mRNA stability or inhibits
328 translation of these isoforms. Consistent with the molecular data, we did not detect any significant
329 changes in the level of Jbug-PC (42.4 kDa) and Jbug-PL (175.6 kDa) in *jbug*^{30} and *jbug*^{133} protein
330 extracts (Figure 1, E and H). Taken together, we generated new alleles for *jbug*, including a null
331 mutant and two hypomorphic alleles that disrupt a subset of Jbug isoforms, specifically Jbug-PI
332 and Jbug-PF/M/N.
333
334 ***jbug* hypomorphs show semi-lethality and defects in bristle development on the thorax**
335 Many homozygous flies in *jbug*^{30} and *jbug*^{133} died during pupation, leaving a number of dead
336 pupae that never eclosed. In both alleles, homozygous adult flies that survived were fertile and
337 homozygous lines could be maintained. Interestingly, adult flies homozygous for *jbug*^{30} or *jbug*^{133}
338 produced short, bent and rough-ended bristles on the thorax (Figure 2A), suggesting a role for
339 Jbug in bristle development, perhaps in crosslinking actin bundles that form the bristles.
340 Consistent with our findings that levels of Jbug-PF/M/N and Jbug-PI were more significantly
341 reduced in *jbug*^{30} than in *jbug*^{133} (Figure 1, E and H), *jbug*^{30} flies showed a higher expressivity of
342 bristle defects than *jbug*^{133}. Whereas almost every thoracic bristle had defects in *jbug*^{30}
343 homozygous adults, only a few bristles showed distinguishable defects in *jbug*^{133} homozygotes
344 (Figure 2A). Phalloidin staining in *jbug*^{30} pupae showed changes in F-actin staining consistent
345 with the bent bristle phenotype (Figure 2B), suggesting that the bristle defects arise during
346 pupation.

347 To analyze the bristle defects in more detail, we performed scanning electron microscopy (SEM)
348 in wild-type and *jbug*^{30} homozygous mutant adults. Whereas wild-type animals showed nicely
349 elongated and tapered bristles that suggested evenly aligned actin bundles (Figure 2C, a and a'),

350 *jbug*^{30} mutant flies had bristles that were short, curved (Figure 2C, c), bent (Figure 2C, d) and
351 rough-ended (Figure 2C, e). Even when the bristles looked relatively normal, they were often
352 shorter than wild type and mildly twisted (Figure 2C; compare b and b' to f and f').

353 Transheterozygotes of *jbug*^{30} or *jbug*^{133} over the *jbug*^{20} null allele or the *59AB* deficiency line that
354 deletes the entire *jbug* gene (Figure 1A) showed both semi-lethality and the same bristle defects
355 as observed in homozygous *jbug*^{30} and *jbug*^{133} adults (Table 1). These data suggest that both
356 phenotypes are due to loss of *jbug* function. Consistent with our data that *jbug*^{30} is a more severe
357 hypomorphic allele than *jbug*^{133} (Figure 1, E and H), fewer transheterozygous *jbug*^{30}/*jbug*^{20} or
358 *jbug*^{30}/*59AB* flies survived to the adult stage compared to transheterozygous *jbug*^{133}/*jbug*^{20} or
359 *jbug*^{133}/*59AB* flies (Table 1). Taken together, these data suggest that Jbug-PF/M/N and/or PI are
360 important for viability and actin bundle arrangement within bristles.

361 We also performed complementation tests using the deficiency line *Exel6079*, which deletes
362 through the genomic region encoding the N-terminal exons of transcripts of *jbug-RL* and *jbug-*
363 *RF/M/N* but leaves the coding region for *jbug-RC* and *jbug-RI* intact (Figure 1A). Interestingly,
364 transheterozygous *jbug*^{30}/*Exel6079* (and *jbug*^{133}/*Exel6079*) flies showed neither semi-lethality nor
365 bristle defects (Table 1). To test which isoforms are present in *jbug*^{30}/*Exel6079* flies, we performed
366 Western blot using extracts from *jbug*^{30}/*Exel6079* transheterozygous 1st instar larvae obtained
367 from *jbug*^{30} homozygous mothers and found that the truncated PI (~90 Kd) band present in *jbug*^{30}
368 is no longer detected; only a full-length PI band is observed in the transheterozygotes. Also
369 surprisingly, the large MW Jbug-PF/M/N bands that were absent/reduced in *jbug*^{30} homozygotes
370 were easily detected in *jbug*^{30}/*Exel6079* larvae (Figure 1G). This finding was unexpected because
371 Jbug-PF/M/N should be absent in transheterozygous *jbug*^{30}/*Exel6079* flies; *jbug*^{30} and *Exel6079*
372 disrupt the 3' and the 5' ends of *jbug-RF/M/N*, respectively. Since *jbug*^{30}/*Exel6079* larvae were
373 obtained from *jbug*^{30} homozygous mothers, Jbug-PI or Jbug-PF/M/N cannot be provided
374 maternally. This result is challenging to reconcile, unless there is some form of transvection or
375 transplicing that would generate full length transcripts coming from the 5' regions of *jbug*^{30} and 3'
376 regions of *Exel6079*. Such events could also explain the recovery of the full-length *jbug-RI*
377 transcript and corresponding loss of the shortened form of Jbug-PI (Figure 1G).
378

379 **Expression of Jbug-RF rescues the bristle defects and semi-lethality of *jbug* hypomorphs**
380 To begin to parse out the functions of the different Jbug isoforms, we created three new UAS
381 lines encoding Jbug-PC (42 kDa protein), Jbug-PI (185.6 kDa) and Jbug-PF (>300 kDa protein).
382 We also obtained a UAS construct for Jbug-PL (175.6 kDa protein) expression from the Mlodzik

383 lab (Olguín *et al.* 2011). We first tested whether expression of any specific *jbug* splice form(s)
384 could rescue the lethality of *jbug*^{20} null mutants. Each UAS construct was expressed in *jbug*^{20}
385 mutant background using *daughterless-Gal4* (*da-Gal4; Wodarz et al., 1995*), which is expressed
386 in all cells, or *69B-Gal4* (Rorth 1996), which is expressed in ectodermal cells. None of the UAS
387 constructs rescued the lethality of *jbug*^{20}; no larvae survived past the 1st instar larval stage as in
388 *jbug*^{20}. Co-overexpression of *jbug-RL* and *jbug-RI* together using da-Gal4 in the *jbug*^{20} mutant
389 background also did not rescue the lethality. These data suggest that multiple Jbug isoforms are
390 required for viability.

391 We next tested whether expression of specific Jbug isoforms could rescue the bristle defects in
392 *jbug*^{30}, the severe hypomorphic allele. Consistent with the data that Jbug-PC is not affected in
393 *jbug*^{30} mutants, overexpression of *jbug-RC* with *da-Gal4* or with *69B-Gal4* in an otherwise wild-
394 type background did not result in any overt defects in bristles (Figure 2D). Overexpression of
395 Jbug-PI in an otherwise wild-type background also did not cause any defects in bristles (Figure
396 2E). On the other hand, overexpression of *jbug-RF* in otherwise wild-type animals resulted in
397 shorter and thicker bristles (Figure 2F), suggesting that proper levels of Jbug-PF/M/N are critical
398 for normal bristle development. Phalloidin staining in *fkh>Jbug-RF* pupae showed the bent bristle
399 phenotype and irregular F-actin alignment, similar to observed in *jbug*^{30} pupal bristles (Figure 2B).
400 Importantly, whereas expression of *jbug-RC* (Figure 2G) or *jbug-RI* (Figure 2H) in *jbug*^{30} mutants
401 did not rescue the bristle phenotypes, expression of *jbug-RF* in *jbug*^{30} mutants using *da-Gal4* or
402 *69B-Gal4* nearly completely rescued the bristle phenotypes (Figure 2I). Moreover, *jbug-RF*
403 expression in *jbug*^{30} mutants also rescued semi-lethality. 86% (27/32) of pupae emerged as adult
404 flies when *jbug-RF* was expressed in *jbug*^{30} mutants, whereas only 26% (9/35) of *jbug*^{30}
405 homozygous pupae emerged as adult flies. These data suggest that the bristle defects and semi-
406 lethality observed in *jbug*^{30} are due to loss of the longest (>300 kDa) Jbug isoforms.
407

408 **Jbug hypomorphs show a delay in actin-based prehair formation and mild defects in wing**
409 **hair orientation**

410 Besides thoracic bristle defects, *jbug*^{30} and *jbug*^{133} homozygous adults also showed a mild swirling
411 pattern of wing hairs (Supplemental Figure 3B and data not shown). Phalloidin staining of actin-
412 rich prehairs at 32 hours after puparium formation (APF) revealed that hair formation is delayed
413 in *jbug*^{30} pupal wings (Supplemental Figure 3, D and E). A swirling pattern of wing hairs and
414 delayed prehair formation are often observed in mutants for planar cell polarity (PCP) genes
415 (Adler 2012). *jbug*^{30} mutant eyes, however, did not have any defects in ommatidial rotation

416 characteristic of loss of key PCP genes (Supplemental Figure 3, F and G), suggesting that Jbug
417 is not involved in ommatidial rotation. Overall, these data suggest that proper levels for Jbug-
418 PF/M/N and/or Jbug-PI are required for the timely maturation of the actin bundles that form the
419 prehairs. In support of this, we find that the wing hair polarity defects are fully rescued in
420 *jbug30/Exel6079* flies (Supplemental Figure 3C).
421
422 **Jbug proteins localize in a dynamic pattern in the embryonic epithelium**
423 We next analyzed the subcellular localization of Jbug proteins during embryogenesis in wild type
424 and *jbug* mutant alleles. During early development, Jbug was detected as small punctate
425 structures in the cytoplasm of all cells (Figure 3, A and B). During stages 11-13, Jbug was
426 detected at a high level both near the apical surface and at and near the adherens junctions (AJs)
427 in all epidermal cells (Figure 3, C and M). AJ Jbug signals became weaker over time, and by
428 stage 15, only mesh-like signals on the apical surface remained (Figure 3, D and M). In $jbug^{20}$
429 mutant embryos, AJ signals were absent, but signals on the apical surface were still detected
430 (Figure 3, E and M). At stage 15 and later, apical surface signals were significantly decreased
431 compared to wild-type levels (Figure 3, F and M). Since the $jbug^{30}$ and $jbug^{133}$ homozygotes that
432 survived to adult stages were fertile, we analyzed Jbug signals in $jbug^{30}$ or $jbug^{133}$ embryos from
433 homozygous mothers. Interestingly, in $jbug^{30}$ embryos from $jbug^{30}$ homozygous mothers, Jbug
434 signals were both very weak and dispersed in epidermal cells throughout the stages and largely
435 absent in AJs (Figure 3, G, H and M), suggesting that Jbug-PF/M/N and Jbug-PI might be major
436 isoforms that show strong embryonic expression and AJ localization. Expression of Jbug-RF in
437 the $jbug^{30}$ mutant background restored strong signals at AJs (Figure 3K) and on the apical surface
438 (Figure 3L) at stage 13 and 15, respectively. Consistent with the minor changes in Jbug protein
439 levels in $jbug^{133}$, Jbug staining was mostly normal, albeit slightly reduced, in the epidermal cells
440 in $jbug^{133}$ embryos from homozygous $jbug^{133}$ mothers (Figure 3, I, J and M).
441
442 **Jbug is required for denticle formation in the epidermis**
443 Jbug antibody staining in the ventral regions of stage 14 embryos revealed intense signals on the
444 apical surface that presaged the actin-rich denticles that begin to form during stage 15 (Figure 4,
445 B and C). This prompted us to ask if denticle formation was normal in *jbug* mutants. In wild-type
446 embryos, six rows of epidermal cells in the anterior portion of each abdominal segment normally
447 produce one or more denticles, forming a trapezoidal belt (Bejsovec 2013; Figure 4, C and D).
448 Embryos homozygous for $jbug^{20}$ did not show any overt morphological defects, likely due to strong
449 maternal contribution, but they exhibited defects in denticle formation (Figure 5B). Compared to

450 wild type (Figure 5A), many denticles in *jbug*^{20} embryos were small and premature (Figure 5B).
451 Also, the overall number of denticles were fewer in *jbug*^{20} embryos compared to wild type. We
452 counted the number of denticles in each cell from a grid of 24 cells (Figure 5K) for at least five
453 individuals of each genotype. *jbug*^{20} embryos had fewer denticles per cell than wild-type embryos
454 in several rows of cells (C1, C3, C4 and C6; Figure 5, L and M; Supplemental Figure 4, A and B).
455 Denticles in *jbug*^{30} embryos from a homozygous stock were relatively normal in their size and
456 morphology, but these embryos had significantly fewer denticles compared to wild type (Fgure
457 5C). Irrespective of which row of cells (C1-C6) was examined, *jbug*^{30} embryos had, on average,
458 fewer denticles per cell than wild-type embryos (Figure 5, L and M; Supplemental Figure 4, A and
459 B). These data suggest important roles of Jbug in actin bundle arrangement for denticle formation.

460 We next tested whether expression of *jbug-RF* or *jbug-RI* rescues the denticle defects in *jbug*^{20}
461 or *jbug*^{30} embryos. Expression of *jbug-RF* using the *da-Gal4* driver in the otherwise wild-type
462 condition did not affect the number of denticles nor the size (Figure 5, F, L and M). Expression of
463 *jbug-RF* using the *da-Gal4* driver in *jbug*^{20} mutants largely restored denticle size (compare Figure
464 5B and 5D), suggesting a role of the Jbug isoforms with actin-binding domains in formation of
465 mature denticles. However, Jbug-RF expression in *jbug*^{20} minimally rescued the decreased
466 denticle number phenotype; it slightly increased the number of denticles in one row (C6), but not
467 significantly in other rows (C1-C5) (Figure 5, D, L and M; Supplemental Figure 4, A and B).
468 Similarly, expression of *jbug-RF* using the *da-Gal4* driver in *jbug*^{30} mutants slightly increased the
469 number of denticles in one row (C1), but not in other rows (C2-C6) (Figure 5, E, L and M;
470 Supplemental Figure 4, A and B). On the other hand, overexpression of *jbug-RI* using the *da-Gal4*
471 driver in the otherwise wild-type condition significantly increased the number of denticles in
472 several rows (C2-C4; Supplemental Figure 4, A and B). In all rows, Jbug-RI-overexpressing
473 embryos have more cells with more than three denticles per cell than wild type (Figure 5L;
474 Supplemental Figure 4, A and B). Moreover, expression of *jbug-RI* using *da-Gal4* in *jbug*^{30}
475 mutants significantly rescued the decreased denticle number phenotype in several rows (Figure
476 5, G, L and M; Supplemental Figure 4, A and B). These data suggest a critical role of Jbug-PI in
477 formation of the actin-rich denticles in the embryo.

478 We further tested whether the maternal pool of *jbug* is required for denticle formation. Knocking
479 down *jbug-RL* and *jbug-RF/M/N* by RNAi (*GD13033*; Figure 1A) using *da-Gal4* also showed
480 similar, albeit weaker, defects to those in *jbug*^{20} embryos: a decrease in the size and numbers of
481 denticles per cell in several rows (Figure 5, I, L and M; Supplemental Figure 4, A and B),
482 suggesting roles for the Jbug isoforms with actin-binding domains in denticle formation. Maternal

483 knockdown of *jbug* using the *matα-Gal4* driver (Häcker and Perrimon 1998) and two strong RNAi
484 lines (*GD8664* and *GD13033*; each targets a subset of *jbug* splice forms; Figure 1A) resulted in
485 very few embryos, suggesting an essential role for Jbug in oogenesis. Maternal knockdown of
486 *jbug* using the weaker RNAi line (*JF01166* that targets all splice forms; Figure 1A) resulted in
487 mostly normal overall embryonic morphology, except for slightly wavy epidermis (Figure 5J), and
488 these embryos showed defects in denticle formation. As observed in *jbug*^{20} and *jbug*^{30} mutants or
489 *da-Gal4>jbug RNAi GD13033* embryos, some cells failed to form denticles; others formed short,
490 premature denticles with weak phalloidin signals (Figure 5, J, L and M). Quantification showed a
491 decrease in the average number of denticles per cell in most columns (except for C2) of each
492 denticle belt with *matα>jbug RNAi* (Figure 5, L and M; Supplemental Figure 4, A and B). Taken
493 together, our data suggest that both maternally and zygotically provided Jbug proteins are
494 required for denticle formation.
495
496 **Jbug is upregulated in embryonic epithelial tubes**
497 Consistent with mRNA expression (BDGP; https://insitu.fruitfly.org/cgi-bin/ex/insitu.pl; Fly-FISH;
498 http://fly-fish.ccbr.utoronto.ca; Supplemental Figure 1), antibody staining in wild-type embryos
499 revealed accumulation of Jbug protein in the trachea and the salivary gland (Figure 6, A and E).
500 Interestingly, Jbug was abundant in both the cytoplasm and in a distinct apical domain of both
501 tracheal and salivary gland cells, which appeared to be just under the apical surface (Figure 6, A
502 and E), as opposed to following the AJ pattern of E-Cad. This apical staining in the salivary gland
503 was prominent up to stage 14; at later stages, Jbug signals were observed mostly in the cytoplasm
504 and detected in the apical domain only as a thin layer along the lumen (compare Figure 6E to
505 Figure 7A).

506 Jbug signals in tubular epithelial organs were significantly decreased in *jbug*^{20} embryos, even with
507 regards to surrounding tissues (Figure 6, B and F), suggesting that zygotic *jbug* expression is
508 required for upregulation of Jbug in these tissues. In *jbug*^{20}, the apical staining in the trachea was
509 absent and in the salivary gland was more punctate. In *jbug*^{30} embryos (from *jbug*^{30} parents),
510 apical staining of Jbug in the trachea and salivary glands was also absent; instead, uniform Jbug
511 signals were detected in the cytoplasm (Figure 6, C and G). Consistent with slight changes in
512 Jbug protein levels in *jbug*^{133}, Jbug signals were mostly normal, albeit slightly reduced, in the
513 trachea and salivary glands in *jbug*^{133} embryos from *jbug*^{133} parents (Figure 6, D and H). These
514 data suggest that it is either the Jbug-PF/M/N and/or Jbug-PI that are enriched in the apical
515 domain in tubular epithelial organs in the embryo.

516 Despite the absence or mislocalization of Jbug in the apical domain of trachea and salivary glands,
517 both organs developed normally without overt morphological defects in *jbug*^{20} and *jbug*^{30} embryos
518 (Figure 6, B, C, F and G). Crumbs (Crb), the apical determinant protein, E-Cadherin (E-Cad), a
519 key adherens junction protein, Discs large (Dlg), a septate junction component, and α-Spectrin
520 (α-Spec), the lateral membrane-associated protein, also localized properly in salivary glands in
521 *jbug*^{20} or *jbug*^{30} embryos (Supplemental Figure 5, A-I), suggesting that the overall epithelial
522 polarity is intact in salivary glands in these mutants. Also, phalloidin signals in salivary glands in
523 *jbug*^{20} and *jbug*^{30} embryos were comparable to wild type (Supplemental Figure 5, D-F), suggesting
524 that F-actin is largely intact in salivary glands in *jbug* mutants.

525 To further test where each of the jbug isoforms localizes and to test the effect of Jbug
526 overexpression in tubular epithelial tissues, we overexpressed the different Jbug isoforms (Jbug-
527 PC, PI, PL and PF) in the salivary gland using the salivary gland-specific *fork head-Gal4* driver
528 (*fkh-Gal4*; Henderson and Andrew 2000). All isoforms primarily localized in the cytoplasm when
529 overexpressed (Figure 7, D-G). Interestingly, however, both untagged and C-terminal GFP-
530 tagged Jbug-PC were detected both in the cytoplasm and in nuclei (Figure 7, B and C). These
531 data suggest that this smallest isoform – which is primarily expressed in pupae (Figure 1E) –
532 might function in the nucleus as well. Similar nuclear localization has been observed with human
533 Filamin A. Although full-length filamin A is predominantly cytoplasmic, a C-terminal fragment of
534 Filamin A colocalizes with the androgen receptor to the nucleus to act as a co-transcription factor
535 (Loy *et al.* 2003). Overexpression of each isoform resulted in an expanded and irregular luminal
536 domain (Figure 7, B-G). Interestingly, Crb was mislocalized and dispersed along the entire apical
537 surface in Jbug-overexpressing salivary glands (Figure 7, B-G) rather than being enriched in a
538 sub-apical domain just apical to the AJs as in control salivary glands (Fig 7A, inset in Crb column;
539 Wodarz *et al.* 1995; Tepass 1996; Chung and Andrew 2014). These data indicate that
540 overexpression of multiple Jbug isoforms can disrupt the sub-apical domain enrichment of Crb.
541 Phalloidin and other junctional and polarity markers, including E-Cad, Nrx-IV (a septate junction
542 marker) as well as α-Spec, localized properly in Jbug-overexpressing salivary glands
543 (Supplemental Figure 6), suggesting that the overall epithelial polarity is not disrupted by Jbug
544 overexpression. Taken together, these data suggest that appropriate levels of Jbug isoforms are
545 important for proper Crb localization and apical organization of epithelial cells during
546 embryogenesis.
547
548 **Jbug is required for maintaining Crb levels in embryonic epithelial cells**

549 Maternal knockdown (*matα>JF01166*) or zygotic loss of all *jbug* splice forms (*jbug*^{20}), or specific
550 maternal and zygotic loss of the *jbug-RF/M/N* and *jbug-RI* (*jbug*^{30}) did not show overt
551 morphological defects in the embryo, except for mild wavy epidermis (Figures 5, B and J) and
552 denticle formation defects (Figure 5). We therefore knocked down both maternal and zygotic pools
553 of all *jbug* splice forms using RNAi. Compared to normal morphology in control embryos (Figure
554 8, A and E) or in embryos knocked down for *jbug* zygotically (using *da-Gal4*; Figure 8, B and F)
555 or maternally (using *matα*-Gal4; Figure 8, C and G), knockdown of *jbug* both maternally and
556 zygotically using *matα-Gal4* and *da-Gal4* (*jbug* MZ knockdown) resulted in a severely disrupted
557 morphology in all embryos produced (Figure 8, D and H). The embryos were often so disrupted
558 that their stages could not be ascertained. Whereas strong Jbug signals were still detected in
559 epithelial cells in embryos knocked down for *jbug* maternally or zygotically (Figure 8, F'' and G'';
560 compare to control in Figure 8E''), Jbug signals were absent in the apical surface in many
561 epidermal cells in *jbug* MZ knockdown embryos (Figure 8H''). Importantly, Crb signals were also
562 absent in those cells (Figure 8H'''). These data suggest a critical role for Jbug in regulating Crb
563 levels and localization in epithelial cells.

564 We also knocked down *jbug* in the salivary gland in embryos also maternally knocked down for
565 *jbug,* using *matα-Gal4* and *fkh-Gal4*. No overt morphological defects were observed in salivary
566 glands in these embryos at stage 11, when the salivary gland begins to invaginate to form a tube
567 (Supplemental Figure 7). However, compared to continuous Crb signals in control or in salivary
568 glands knocked down for *jbug* maternally or zygotically only, huge gaps in Crb signals were
569 detected in salivary glands in *jbug* MZ knockdown embryos (Supplemental Figure 7, A''''-D''''). At
570 later stages, knockdown of *jbug* resulted in a slightly irregular salivary gland lumen (Figure 8, I-
571 M). Importantly, compared to the continuous sub-apical localization of Crb in control or SG cells
572 with zygotic knockdown for *jbug*, the salivary glands knocked down for *jbug* maternally showed
573 discontinuous Crb signals (Figure 8I'''). Salivary glands knocked down for *jbug* both maternally
574 and zygotically showed reducted Crb signals with wider gaps (Figure 8L''') or mislocalization of
575 Crb signals to the apical surface (Figure 8M'''). Overall, these data reveal that Jbug is required
576 for proper levels and distribution of Crb in epithelia.
577

578 **Discussion**

579 Filamins play important roles in actin reorganization in many developmental processes and
580 disease contexts. In this study we show that different isoforms of Jbug, a *Drosophila* filamin-type
581 protein, are differentially expressed and localized during development. Using new genetic tools
582 that we generated, we reveal essential roles for different Jbug isoforms in viability, epithelial
583 morphogenesis and formation of actin-rich structures.

584

585 **Roles of different Jbug isoforms in various developmental stages in *Drosophila***

586 Our developmental western analysis (Figure 1), along with developmental RNA-Seq data by
587 Flybase (www.flybase.org; FB2021_02), reveals differential expression of different Jbug isoforms
588 throughout development. Although transcripts of isoforms containing actin-binding domains (*jbug-*
589 *RF/M/N* and *jbug-RL*) are not expressed until several hours of embryogenesis, proteins for these
590 isoforms are detected at early hours of embryogenesis, suggesting Jbug proteins are provided
591 maternally. Our studies reveal roles of different Jbug isoforms at various developmental
592 processes, including oogenesis, epithelial morphogenesis, and viability at larval and pupal stages.

593 Severe defects in egg laying upon maternal knockdown of *jbug* using two strong RNAi lines that
594 target a different subset of isoforms (*GD13033* and *GD8664*) suggest critical roles for Jbug
595 isoforms in oogenesis. *GD13033* targets Jbug-PF/M/N and Jbug-PL, suggesting roles for the
596 actin-binding domain-containing isoforms in oogenesis. Homozygous $jbug^{30}$ flies can be
597 maintained as a homozygous stock depite the apparent absence of Jbug-PF/M/N and truncated
598 Jbug-PI, suggesting that these Jbug isoforms do not play an essential role in oogenesis. Since
599 Jbug-PC is only made in pupae, the main isoform for oogenesis is likely to be Jbug-PL (Figure 9).

600 Our study also reveals a critical role of Jbug in epithelial morphogenesis during embryogenesis.
601 Embryos knocked down for *jbug* both maternally and zygotically show severe morphological
602 defects with disrupted Crb localization (Figure 8). The precise mechanism underlying Crb
603 regulation by Jbug remains to be discovered. As filamin binds to many interacting proteins via IG-
604 FLMN repeats, it will be interesting to test whether Jbug regulates Crb by directly interacting with
605 it. It is also possible that Crb reduction is an indirect effect of disrupted actin cytoskeleton by loss
606 of Jbug. Dynamic localization of Jbug isoforms to the apical surface during embryogenesis
607 (Figures 3 and 4) suggests potential roles for different Jbug isoforms in remodeling the actin
608 cytoskeleton and contributing to the mechanical stability of the plasma membrane and the cell
609 cortex. Interestingly, homozygous $jbug^{30}$ embryos from homozygous mothers, where only Jbug-
610 PC and Jbug-PL are intact, show no overt defects during embryogenesis except for defects in

611 denticle formation at later stages (Figure 5). As Jbug-PC is not expressed during embryogenesis
612 (Figure 1), these data indicate that Jbug-PL is largely sufficient for epithelial morphogenesis
613 during embryogenesis (Figure 9).

614 Jbug is also required for viability. The *jbug*^{20} null allele lacking all Jbug isoforms is 1st instar larval
615 lethal. 1st instar larvae of homozygous *jbug*^{20} or transheterozygous animals of *jbug*^{20} and a
616 deficiency line appear normal in their overall size, morphology and motility, but they do not molt
617 into the 2nd instar. Based on the role of Jbug in regulating Crb localization during embryogenesis
618 (Figures 7 and 8), the lethality of *jbug*^{20} homozygous larvae might be linked to disruption of Crb
619 localization and/or epithelial organization during the larval stage. As overexpressing a single
620 isoform or Jbug-RL and Jbug-RI together failed to rescue the lethality of *jbug*^{20}, multiple Jbug
621 isoforms may be required for viability during early stages of development.

622 Our *jbug* hypomorphic alleles reveal roles for Jbug-PF/M/N and/or Jbug-PI in organismal viability
623 late in development (Table 1). Most flies homozygous for *jbug*^{30} or *jbug*^{133}, or transheterozygous
624 flies for these *jbug* alleles and a deficiency completely removing *jbug* die during late pupation.
625 Jbug-PF expression in the *jbug*^{30} mutant background rescued this semi-lethality, suggesting that
626 the longest splice forms (PF/M/N) are required at these late stages. Interestingly, anatomy RNA-
627 Seq by Flybase (www.flybase.org; FB2021_02) shows increased *jbug* expression in the fat body
628 at pupal stage P8 (2 days old; moderate levels of expression) compared to the white prepupae
629 stage (very low expression), opening up the possibility for a role for Jbug in the fat body. The fat
630 body of *Drosophila* is equivalent to vertebrate adipose tissue and liver in its storage and major
631 metabolic functions, including immune response and sensing nutritional conditions. It remains to
632 be revealed whether the lethality caused by the loss (or significant reduction) of Jbug-PF/M/N is
633 related to defects in morphogenesis, metabolic functions, or both.
634

635 **Jbug plays a role in formation of actin-rich protrusions**

636 Our results identify roles for specific Jbug isoforms in formation of two prominent actin-rich
637 protrusions in *Drosophila*, bristles on the thorax and denticles in the ventral epidermis of the
638 embryo (Figures 2 and 5). Jbug may regulate assembly of actin bundles by interacting with actin-
639 regulating proteins, such as capping protein and the Arp2/3 complex components. Mutants for
640 capping protein or the Arp2/3 complex components show bristle defects reminiscent of the *jbug*
641 mutant phenotypes (Hudson and Cooley 2002; Frank *et al.* 2006). Several studies in other
642 systems also suggest that the Arp2/3 complex synergizes with filamins. In filamin-deficient
643 melanoma cells, the Arp2/3 complex is still abundant but unable to stabilize the plasma

644 membranes or support locomotion (Cunningham *et al.* 1992). Also, branched actin filaments
645 made with Arp2/3 do not have the closing loop structures necessary to form three-dimensional
646 structures (Mullins *et al.* 1998; Blanchoin *et al.* 2000), unless the filaments are assembled in the
647 presence of filamin (Niederman *et al.* 1983; Wolosewick and Condeelis 1986). Other good
648 candidates that might interact with Jbug to organize the actin cytoskeleton include the Rho family
649 small GTPases and their regulators. The Rho family small GTPases, including Rho, Rac, and
650 Cdc42 are known to physically interact with Filamin (Ohta *et al.* 1999; Jeon *et al.* 2008; Del Valle-
651 Pérez *et al.* 2010), as are regulators of Rho GTPases, including guanine nucleotide exchange
652 factors (Bellanger *et al.* 2000; Pi *et al.* 2002), GTPase activating proteins (Ohta *et al.* 2006;
653 Mammoto *et al.* 2007; Nakamura *et al.* 2009) and Rho kinase (Ueda *et al.* 2003). It will be
654 interesting to test whether Jbug works with any of these proteins to regulate bristle and/or denticle
655 formation.

656 Defects in actin-rich protrusions in *jbug*^{30} are observed in the presence of Jbug-PL, which contains
657 actin-binding domains and short IG-FLMN repeats, suggesting that this isoform is not sufficient to
658 form normal bristles and denticles in *Drosophila*. Indeed, bristle defects are rescued by expression
659 of Jbug-PF, one of the longest isoforms that contain long IG-FLMN repeats following the actin-
660 binding domains (Figure 2). <u>These data suggest an important role for protein interactions through</u>
661 <u>the long IG-FLMN repeats in forming actin-rich protrusions</u>. Our interpretation is consistent with a
662 role of filamins in acting as a molecular scaffold. More than 90 filamin-binding partners have been
663 identified, including intracellular signaling molecules, receptors, ion channels, transcription factors,
664 and cytoskeletal and adhesion proteins (Razinia *et al.* 2012).

665 Surprisingly, <u>defects in denticle numbers in *jbug*^{30} embryos are rescued by expression of Jbug-</u>
666 <u>PI</u>, an isoform that contains long IG-FLMN repeats without the actin-binding domains, but only
667 minimally by expression of Jbug-PF (Figure 5). These data suggest a major role of Jbug-PI in
668 denticle formation (Figure 9). Although Jbug is upregulated in the anterior side of each segment
669 in the embryo, where denticle belts form, Jbug is not enriched in the denticles themselves (Figure
670 4). Interestingly, another *Drosophila* filamin – Cher – is enriched in denticles, colocalizing with
671 actin protrusions (Dilks and DiNardo 2010). The different subcellular localization of Jbug and Cher
672 in denticle forming cells suggests distinct roles for the two *Drosophila* filamins. Cher likely acts as
673 a component of denticles that organizes actin filaments. A simple model for Jbug function is that
674 actin-binding domains might act to stabilize actin filaments and that protein-protein interactions
675 through long IG-FLMN repeats might recruit other key components for denticle formation to the
676 apical plasma membrane where actin-rich protrusions arise. Still, Jbug-RF/M/N and/or Jbug-RL

677 appear to contribute to denticle formation. Although overexpression of *jbug-RF* in *jbug*^{20} or *jbug*^{30}
678 mutant embryos does not fully rescue the decrease of denticle numbers (Figure 5), zygotic
679 knockdown of *jbug-RF/M/N* and *jbug-RL* using the RNAi line specifically targeting them (*GD13033*)
680 results in premature/small denticle formation and also decreases the number of denticles in some
681 rows (Figure 5), suggesting roles for the actin-binding domain-containing isoforms in denticle
682 formation (Figure 9).
683
684 **Jbug is likely to affect PCP indirectly**
685 *jbug*^{30} and *jbug*^{133} alleles show a delay of actin-rich prehair formation in the pupal wing and a mild
686 swirling pattern of adult wing hairs (Supplemental Figure 3). Both phenotypes are often shown in
687 mutants of PCP genes (Adler, 2002). *jbug* mutants, however, do not show any defects in
688 ommatidial rotation, suggesting that Jbug is less likely to directly affect the core PCP pathway.
689 Rather, the phenotypes in pupal/adult wing hairs are likely to be caused by defects in formation
690 of actin protrusions, similar to what we observe in thoracic bristles (Figure 2) and denticles (Figure
691 5) in *jbug* mutants. Consistent with this idea, Jbug has been proposed to modulate the mechanical
692 properties of actin filaments in tendon cells to regulate planar orientation of thoracic bristles;
693 alterations in the ability to adjust tensile forces upon *jbug* knockdown disrupt the planar orientation
694 of bristles (Olguin et al., 2011).
695
696 **Roles of Jbug in formation of tubular organs**
697 Several studies suggest roles for filamin A in tubular epithelial morphogenesis and diseases in
698 tubular organs. During branching morphogenesis of mammary glands, the levels of filamin A
699 expression and the extent of the integrin-filamin interaction modulate collagen remodeling to
700 optimize matrix stiffness to support tubulogenesis (Gehler *et al.* 2009). Filamin A is also an
701 important regulator for Polycystin-2, a key molecule in autosomal polycystic kidney disease
702 (Wang *et al.* 2015). Our data also suggests a role for Jbug in apical domain reorganization in
703 tubular epithelial cells (Figures 7 and 8). Jbug shows strong apical enrichment in the early
704 embryonic trachea and the salivary gland (Figure 6) and both Jbug loss and overexpression cause
705 defective tube morphology with disrupted Crb localization along the apical surface of salivary
706 gland cells (Figures 7 and 8). These data support the idea that appropriate levels of Jbug are
707 important for apical organization during tubular organ development. Loss of apical Jbug
708 enrichment, however, does not cause overt defects in tubular organ formation in *jbug* null or
709 hypomorphic alleles (Figure 6). In these alleles, abundant cytoplasmic Jbug signals still remain,
710 and the levels or distribution of Crb was not noticeably changed (Supplemental Figure 5).

711 Overexpressed Jbug also mainly localizes to the cytoplasm in salivary gland cells, with only slight
712 apical enrichment (Figure 7). These data suggest that apical enrichment may not be necessary
713 for Jbug function in the formation of tubular epithelia.
714
715 **Transvection or trans-splicing might occur in the *jbug* locus**
716 The surprising rescue that we have observed of viability, bristle morphology and wing hair
717 orientation of *jbug*^{30} and to a lesser extent with *jbug*^{133} with *Exel6079*, a deficiency that deletes
718 all *jbug* exons upstream of the transcription start sites of *RC* and *RI* (Table 1; Supplemental Figure
719 3), suggests epigenetic regulation. One possible mechanism is transvection, an epigenetic
720 phenomenon that results from interactions between alleles on homologous chromosomes in
721 tissues where the chromosomes are paired (King *et al.* 2019), typically with enhancers of one
722 allele on one chromosome affecting expression of the other allele on the homologous
723 chromosome. Here, however, we have to propose transvection via template-switching, wherein
724 transcripts from the *jbug*^{30} allele would switch templates at some point outside the *Exel6079*
725 deficiency but before the large insertion in *jbug*^{30}, for example. Another possibility is trans-splicing,
726 a gene regulatory mechanism that joins exons from two separate transcripts to produce chimeric
727 mRNA, and has been detected in most eukaryotes (Horiuchi and Aigaki 2006; Lasda and
728 Blumenthal 2011). In *Drosophila*, trans-splicing has been demonstrated to be an essential
729 process for two genes, *longitudinals lacking* (*lola*) and *modifier of mdg4* (*mod(mdg4)*). In the *lola*
730 locus, the 5'-end of *lola* transcripts contain five exons that splice into 20 variants of 3' exons to
731 generate 20 protein isoforms (Ohsako *et al.* 2003). In the *mod(mdg4)* locus, two mutant alleles of
732 the gene, each located in one of the two homologous chromosomes, restore the wild-type function
733 of the gene (Mongelard *et al.* 2002), much like is observed here. The presence of Jbug-PF/M/N
734 isoforms (and the rescue of PI size) in transheterozygous animals for *jbug* hypomophs and
735 *Exel6079* (Figure 1G) supports the idea that trans-splicing might occur, where the 5' exons of
736 *jbug-RF/M/N* transripts on *jbug*^{30} or *jbug*^{133} are spliced to 3' exons of *jbug* transcripts on the
737 *Exel6079* chromosome. Recent studies have revealed conserved sequences in the *mod(mdg4)*
738 intron that promote trans-splicing in this gene (Gao *et al.* 2015; Tikhonov *et al.* 2018). Identification
739 of the sequences that promote trans-splicing in the *jbug* locus will help better understand this
740 surprising gene regulatory mechanism.
741

742 **Table 1. Complementation test**

743

	Number of Progeny	
	CyO	Non-CyO
jbug^{20}*/CyO* x *jbug*^{20}*/CyO*	>200	0
jbug^{20}*/CyO* x *Df(2R)59AB/CyO*	>200	0
jbug^{20}*/CyO* x *Df(2R)Exel6079/CyO*	>200	0
jbug^{30}*/CyO* x *jbug*^{20}*/CyO*	176	12*
jbug^{30} (F) x *jbug*^{20}*/CFL* (M)	144	50*
jbug^{30}*/CyO* x *Df(2R)59AB/CyO*	231	41*
jbug^{30}*/CyO* x *Df(2R)Exel6079/CyO*	98	91
jbug^{133}*/CyO* x *jbug*^{20}*/CyO*	141	62*
jbug^{133} (F) x *jbug*^{20}*/CFL* (M)	64	70*
Jbug^{133}*/CyO* x *Df(2R)59AB/CyO*	153	47*
jbug^{133}*/CyO* x *Df(2R)Exel6079/CyO*	140	100
* Transheterozygous flies show the same bristle defects as *jbug*^{30} or *jbug*^{133} homozygotes (See Figure 2 for phenotypes in homozygotes).		

744

745 **Figure legends**

746 **Figure 1. Differential expression of Jbug isoforms throughout *Drosophila* development and**
747 **generation of null and hypomorphic alleles of *jbug*.** (A) Ten annotated splice forms of *jbug*
748 are reported by FlyBase. Deletion regions for two deficiency lines in the *jbug* locus and the $jbug^{20}$
749 null allele are indicated. Cyan bars, three RNAi lines for *jbug* that were tested in this study.
750 Magenta bar, a common exon for all isoforms that was used to generate an antibody against Jbug.
751 Light green bars, regions used for making antisense probes for in situ hybridization. (A', A'')
752 Molecular alterations in two hypomorphic alleles of *jbug*. Blue and red boxes represent homology
753 arms that were used for homologous recombination. Genomic sequence locations are shown for
754 the homology arms. Hypomorphic alleles were generated by incomplete homologous
755 recombination, with a partial ($jbug^{30}$, A') or a complete ($jbug^{133}$, A'') insertion of the donor DNA
756 into the *jbug* isoforms that have a longer C terminus (*RF/M/N* and *RI*). (B) Six different Jbug
757 protein isoforms are made from the different annotated splice forms. (C) Developmental RNA-
758 Seq data by Flybase (www.flybase.org; FB2021_02). Note that only minimal expression of *jbug-*
759 *RF/M/N* and *jbug-RL* is detected until 10 hours of embryogenesis (red arrow). (D-F) Western blot
760 using protein extracts from wild type and *jbug* mutants at different stages. Bands that correspond
761 to the predicted molecular weights of several isoforms are marked with dots and arrowheads with
762 different colors. Arrowheads of the same colors are used to indicate the major isoforms in B. (D)
763 Developmental western blot using protein extracts from embryos (0-2 and 2-16 hours AEL at
764 25°C), 1st, 2nd and 3rd instar larvae, pupae (2 days APF) and male (M) and female (F) adults (2
765 days post-eclosion). (E) Western blots using protein extracts from different *jbug* mutants.
766 Asterisks, two small bands that are still observed in $jbug^{20}$ larvae, which are likely from nonspecific
767 cross-reactivity. (F) In both *59AB* and *Exel6079* homozygous embryos, the same protein bands
768 are detected as in wild type. Note that two faint but distinct bands are visible for >300 KDa,
769 suggesting that Jbug-PM (306.1 kDa) and the other two bigger isoforms, Jbug-PF (318.9 kDa)
770 and Jbug-PN (322.7 kDa), are separated in this gel. (J) In $jbug^{30}$*/Exel6079* transheterozygous
771 larvae, Jbug-PF/M/N, Jbug-PI and Jbug-PL bands are all detected. (H) Protein levels of Jbug
772 isoforms in each *jbug* mutant. Each mutant's viability is also shown.
773

Figure 1

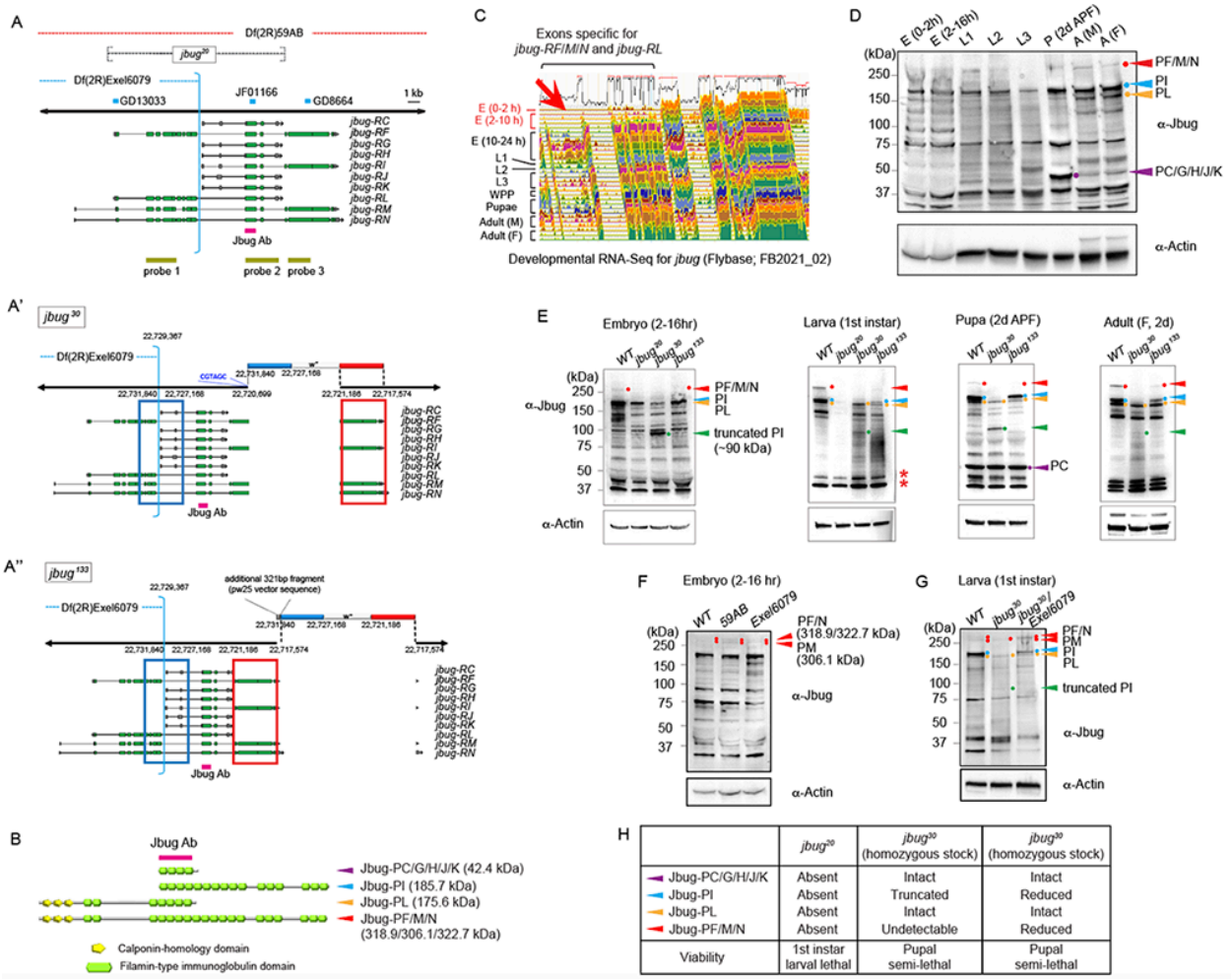

H

	jbug^{20}	*jbug*^{30} (homozygous stock)	*jbug*^{30} (homozygous stock)
Jbug-PC/G/H/J/K	Absent	Intact	Intact
Jbug-PI	Absent	Truncated	Reduced
Jbug-PL	Absent	Intact	Intact
Jbug-PF/M/N	Absent	Undetectable	Reduced
Viability	1st instar larval lethal	Pupal semi-lethal	Pupal semi-lethal

776 **Figure 2. *jbug*^{30} and *jbug*^{133} show bristle defects on the adult thorax, which are rescued by**
777 **expression of Jbug-RF.** (A) Compared to wild type, *jbug*^{30} and *jbug*^{133} adult flies show distinct
778 thoracic bristle defects, including short bristles with rough ends and bent bristles (arrowheads).
779 *jbug*^{133} flies have milder defects than *jbug*^{30}. (B) Phalloidin staining (red) shows the bent bristle
780 phenotype in *jbug*^{30} and *da>Jbug-RF* pupae (arrows) compared to the straight wild-type bristle.
781 (C) SEM images for bristles in wild-type and *jbug*^{30} male flies. Bristles in the red and yellow boxes
782 on the flies are shown in higher magnification in a-f. Compared to the nicely elongated and tapered
783 wild-type bristle (a), bristles in *jbug*^{30} mutants are short and distorted (c), bent (d), and rough-
784 ended (e). Even when the bristle looks relatively normal, it is often shorter than the wild type and
785 slightly twisted (compare b and f). (a'-f') Higher magnification of a-f is shown. (D-F) Whereas
786 overexpression of Jbug-RC (D) or Jbug-RI (E) using *69B-Gal4* or *da-Gal4* in an otherwise wild-
787 type animal does not cause overt defects in thoracic bristles, overexpression of Jbug-RF causes
788 short thick bristles (F; red arrowheads). (G-I) Although expression of Jbug-RC (G) or Jbug-RI (H)
789 does not rescue the bristle defects in *jbug*^{30} (red arrowheads), Jbug-RF expression almost
790 completely rescues the bristle defects in *jbug*^{30}, leaving only a couple of short bristles (I; cyan
791 arrowheads).
792

Figure 2

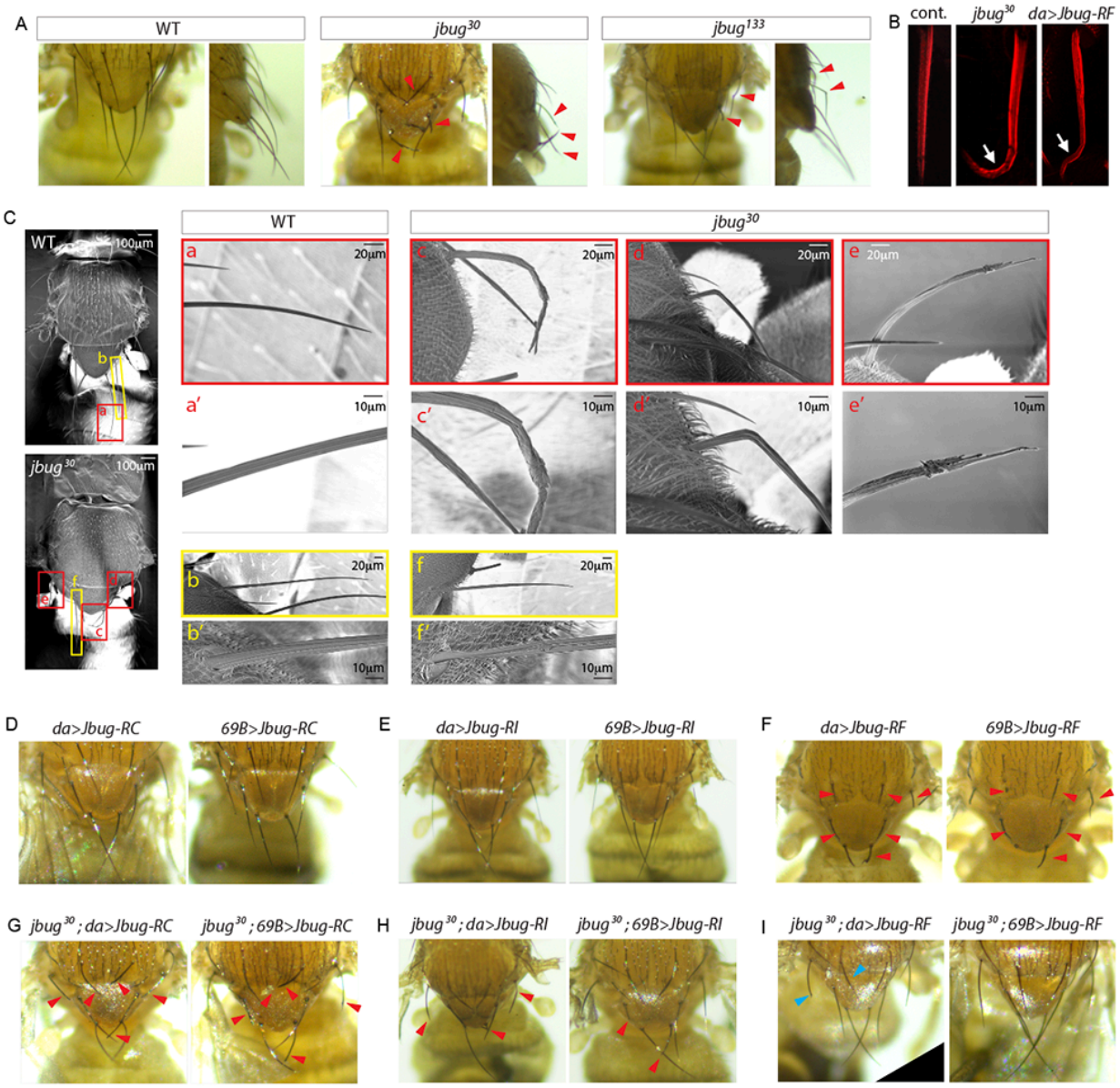
A
WT
jbug30
jbug133
B
cont.
jbug30
da>Jbug-RF
C
WT
jbug30
100µm
20µm
10µm
a
a′
b
b′
c
c′
d
d′
e
e′
f
f′
D
da>Jbug-RC
69B>Jbug-RC
E
da>Jbug-RI
69B>Jbug-RI
F
da>Jbug-RF
69B>Jbug-RF
G
jbug30;da>Jbug-RC
jbug30;69B>Jbug-RC
H
jbug30;da>Jbug-RI
jbug30;69B>Jbug-RI
I
jbug30;da>Jbug-RF
jbug30;69B>Jbug-RF

795 **Figure 3. Analysis of Jbug protein localization in the embryonic epidermis in different *jbug***
796 **alleles.** (A, B) Confocal images for early embryos stained for Jbug (green) and phalloidin
797 (magenta). Jbug localizes as small apical punctate structures. (C-L) Confocal images for
798 epidermis in stage 13 (C, E, G, I, K) and stage 15 (D, F, H, J, L) embryos stained for Jbug (green)
799 and E-Cad (magenta). (C, D) In wild type, whereas high Jbug signals are observed both on the
800 apical surface (arrowheads) and at adherens junctions (arrows) at stage 13 (C), Jbug mostly
801 localizes more uniformly across the apical surface (arrowheads) at stage 15 (D). (E, F) In *jbug*^{20}
802 mutants, junctional Jbug signals are absent, and signals on the apical surface are weak
803 (arrowheads in E). (G, H) In *jbug*^{30} mutants, overall Jbug signals are very weak and diffused
804 throughout the stages. (I, J) In *jbug*^{133} embryos, signals at both the apical surface (arrowheads)
805 and junctions (arrows) are present but are slightly weaker than wild type. (K, L) Jbug-RF
806 overexpression in ectodermal cells driven by *69B-Gal4* in the *jbug*^{30} mutant background (K)
807 results in upregulation of Jbug signals in the entire apical domain with junctional enrichment at
808 stage 13 (arrows). Overexpression of Jbug-RF in all cells by *da-Gal4* in the *jbug*^{30} mutant
809 background (L) causes upregulation of Jbug signals in the apical domain at stage 15 (arrowheads).
810 (M) A summary of Jbug protein localization in the embryonic epidermis in wild type and *jbug*
811 mutant alleles.
812

Figure 3

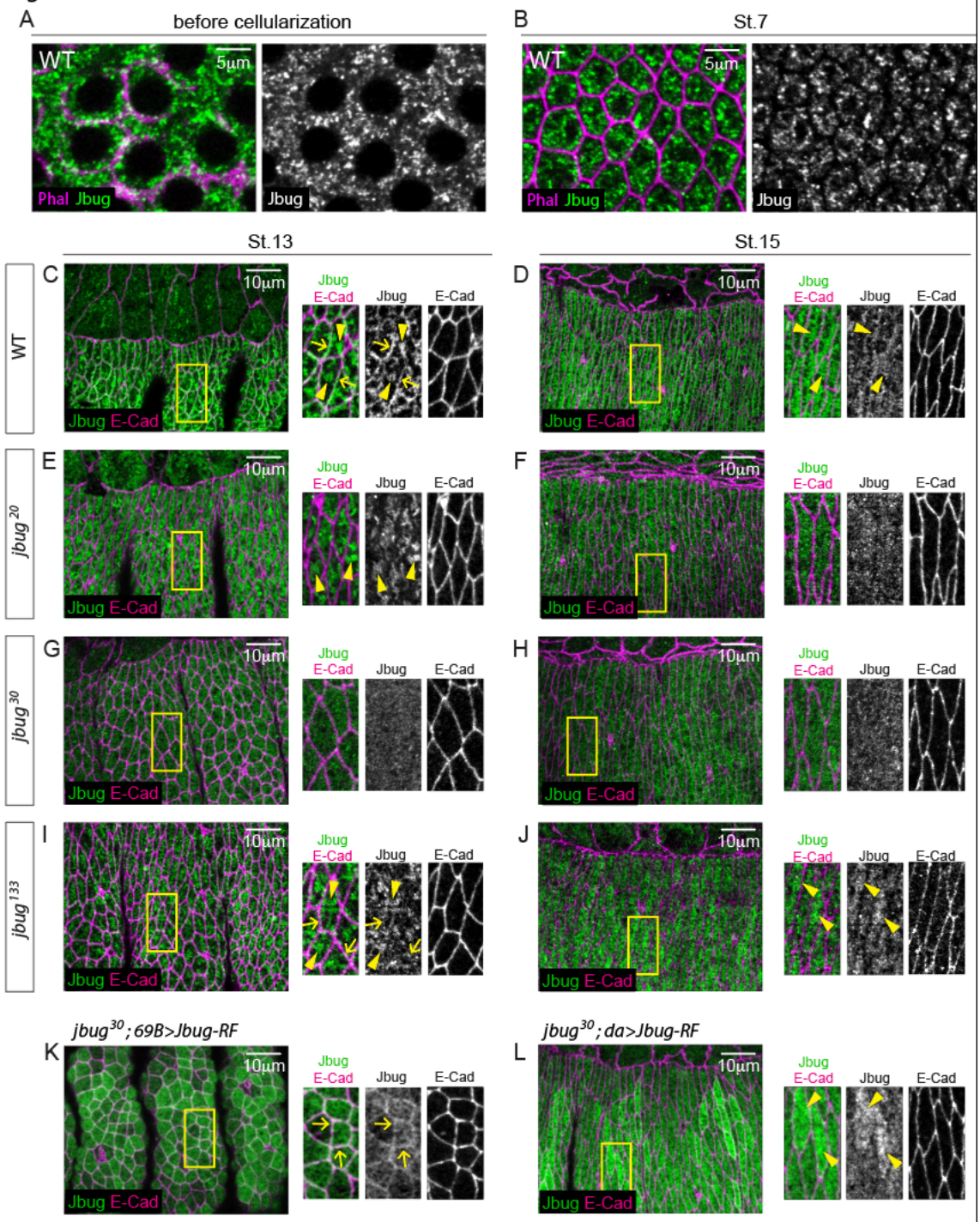

M

	WT	*jbug*^{20}	*jbug*^{30} (homozygous stock)	*jbug*^{133} (homozygous stock)
St. 13	Apical surface & Junctions	Apical surface (weak)	Weak and diffuse	Apical surface & Junctions
St. 15	Apical surface	Apical surface (weak)	Weak and diffuse	Apical surface

814 **Figure 4. Jbug protein is upregulated in the anterior part of each segment just prior to the**
815 **formation of actin-rich denticles in the same region.** (A-D) Epidermis in stages 13 (A), 14 (B),
816 15 (C) and 16 (D) embryos stained for Jbug (green), phalloidin (red), and E-Cad (magenta). (A)
817 At stage 13, Jbug is mostly uniform across epidermis. (B) At stage 14, actin begins to be
818 upregulated in the anterior side of each segment. Jbug also shows accumulation in the apical
819 domain of epidermal cells in the anterior side of the segment. (C-D) At stages 15 (C) and 16 (D),
820 actin-rich denticles form in the anterior side of each segment. Jbug still shows higher levels in
821 those regions. A and P represent the anterior and the posterior side, respectively.
822

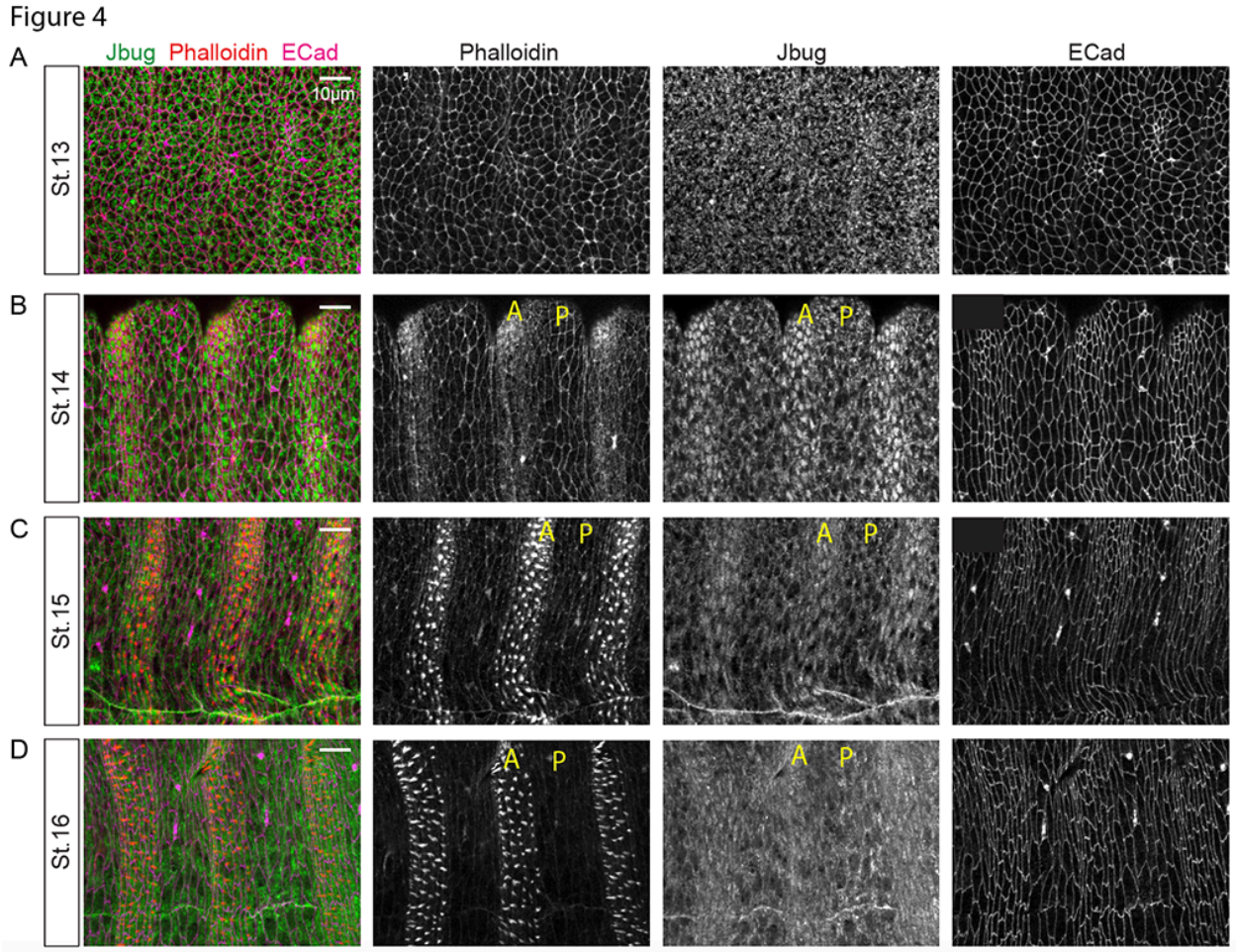

823 **Figure 5. Jbug regulates the formation of denticle precursors in the ventral epidermis of**
824 **the embryo.** (A-G) Stage 16 embryos stained for E-Cad (magenta; cell boundaries) and phalloidin
825 (green; denticles). Ventral epidermis in wild type (A), *jbug*^{20} (B), *jbug*^{30} (C), *jbug*^{20} ; *da-Gal4>Jbug-*
826 *RF* (D), *jbug*^{30} ; *da-Gal4>Jbug-RF* (E), *da-Gal4>Jbug-RF* (F), *jbug*^{30} ; *da-Gal4>Jbug-RI* (G), *da-*
827 *Gal4>Jbug-RI* (H), *da-Gal4>jbug RNAi* (*GD13033*) (I) and *matα-Gal4>jbug RNAi* (*JF01166*) (J) is
828 shown. (A) Epidermal cells at the denticle belt in the abdominal segment 5 (yellow box) are shown
829 at higher magnification. Dotted yellow line, ventral midline. (B-J) Epidermal cells of the same
830 region as in A are shown. For all the embryos, anterior is to the left. (B, J) *jbug*^{20} mutants (B) and
831 *matα-Gal4>jbug RNAi* embryos (J) show mild defects in the embryo morphology, such as wavy
832 epidermis (areas with dotted lines; cells are out of focus). Occasionally, cells either fail to form
833 denticles (arrow in J) or form very short denticles (arrowheads in B, I and J). (K) A cartoon for
834 quantification of the denticle numbers. Four cells that are closest to the ventral midline were
835 chosen in each of the six columns of cells in denticle belts in abdominal segments 4, 5 and 6
836 (column 1, most anterior). (L) Percentage of cells that have different numbers of denticles in C1
837 and C6. See Supplemental Figure 4 for quantification for C2-C5. (M) Quantification of the average
838 number of denticles per cell in C1 and C6. Student's t-test with Welch's correction is used for
839 statistics calculation. (O) A summary of denticle defects in *jbug* mutant alleles and RNAi
840 knockdown and rescue results with Jbug-RF and -RI.
841
842

Figure 5

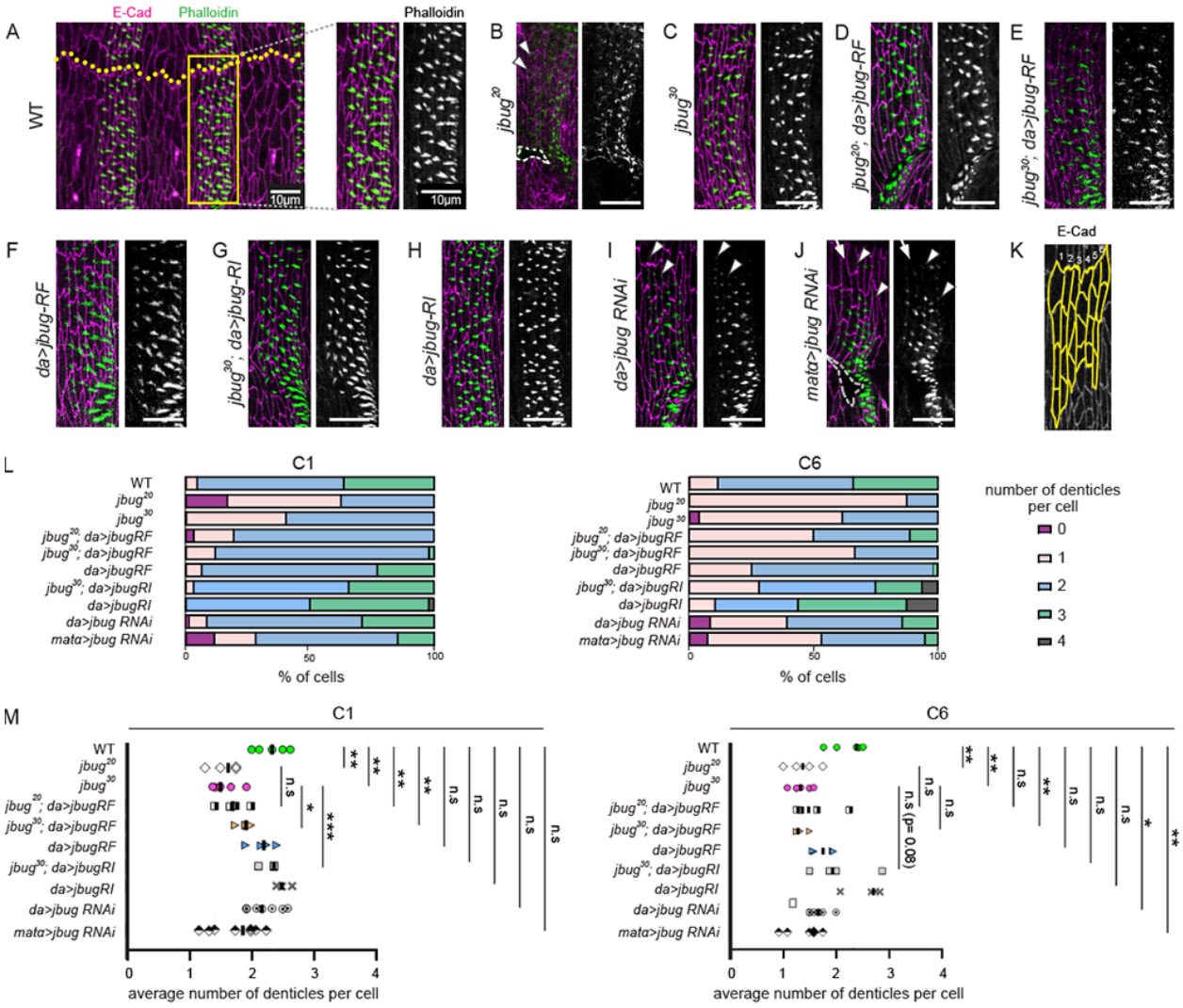

O

	jbug^{20}	*jbug*^{30} (homozygous stock)	*jbug* RNAi zygotic (*jbug* splice forms w/ ABDs)	*jbug RNAi* maternal (all *jbug* splice forms)
Denticle size	Small, Premature (Rescued by RF)	Normal	Small, premature	Small, premature
Denticle numbers	Fewer denticles in some rows (Minimal rescue by RF)	Fewer denticles in all rows (Minimal rescue by RF; Significant rescue by RI)	Fewer denticles in some rows	Fewer denticles in some rows

845 **Figure 6. Jbug protein is apically enriched in the embryonic trachea and the salivary gland,**
846 **and this enrichment is absent in *jbug*^{20} and *jbug*^{30} mutants.** (A-D) Confocal images of stage
847 14 embryonic trachea stained for Jbug (green) and E-Cad (magenta). (A) In wild type, weak Jbug
848 signals are observed in all tracheal cells, with enrichment in the apical domain (arrowheads). (B)
849 In *jbug*^{20} embryos, Jbug signals in the trachea are mostly absent (arrows). (C) In *jbug*^{30} mutant
850 embryos, Jbug signals are diffused in the cytoplasm in tracheal cells (asterisks), with no apical
851 enrichment (arrows; compare to E-Cad signals (arrowheads) in the apical domain). (D) In *jbug*^{133},
852 apical enrichment of Jbug is still present (arrowheads). (E-H) Stage 14 salivary glands stained for
853 Jbug (green) and E-Cad (magenta). (E) Similar to tracheal signals, Jbug is enriched in the apical
854 domain of wild-type salivary gland cells (arrowheads) with weak signals in the cytoplasm. (F) In
855 *jbug*^{20}, overall Jbug signals are significantly decreased in the salivary gland and apical enrichment
856 is mostly gone (arrow; compare to E-Cad signals (arrowhead) in the apical domain). (G) In *jbug*^{30},
857 Jbug is not apically enriched in the salivary gland (arrow; compare to E-Cad signals (arrowhead)
858 in the apical domain) but diffused in the cytoplasm. (H) In *jbug*^{133}, apical enrichment of Jbug is still
859 present (arrowheads). (I) A summary of Jbug protein localization in the trachea and the salivary
860 gland in wild type and *jbug* mutant alleles.
861

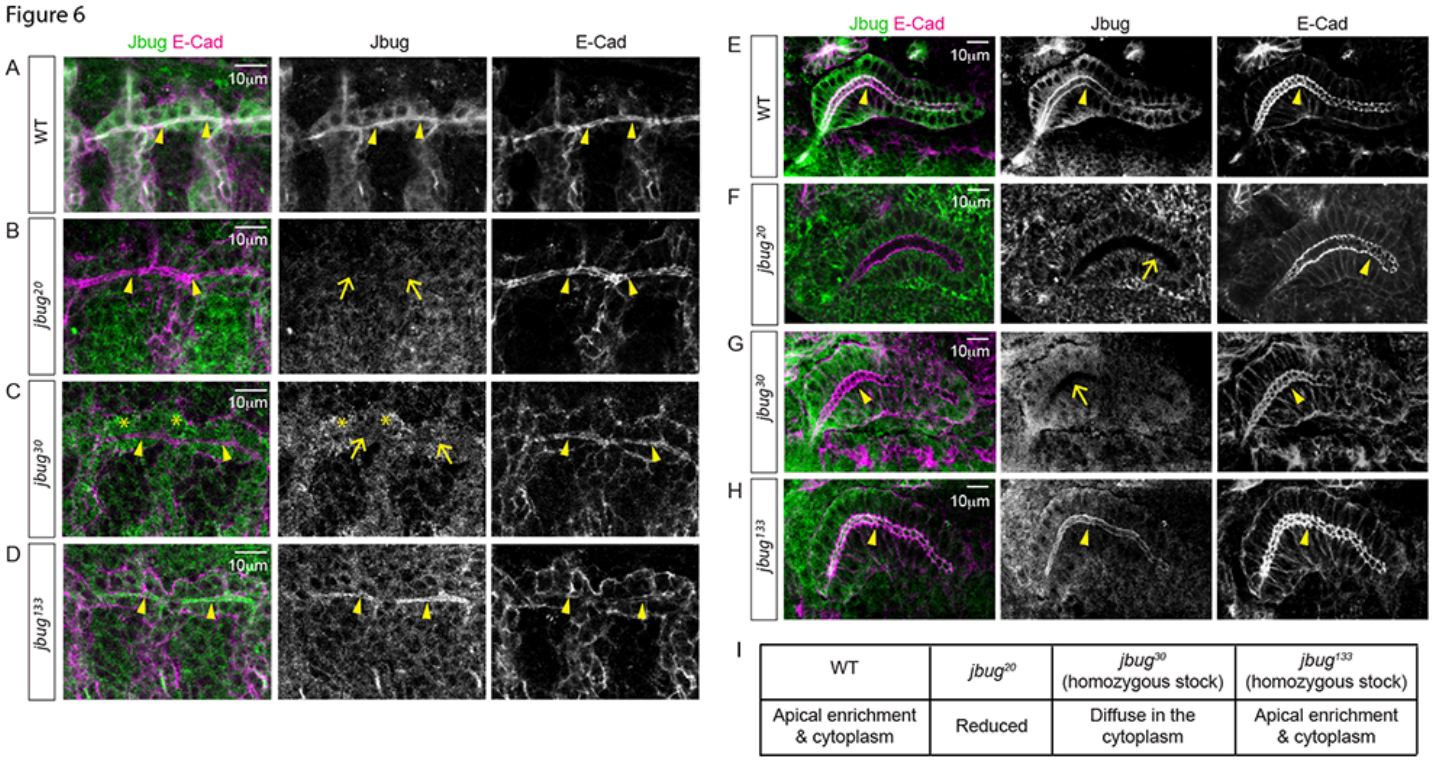

WT	*jbug*^{20}	*jbug*^{30} (homozygous stock)	*jbug*^{133} (homozygous stock)
Apical enrichment & cytoplasm	Reduced	Diffuse in the cytoplasm	Apical enrichment & cytoplasm

862 **Figure 7. Jbug overexpression in the salivary gland causes mislocalization of Crb along**
863 **the apical surface and an expanded and irregular apical domain.** (A-D) stage 16 salivary
864 glands stained for Crb (green), Jbug (magenta), GFP (magenta in C) and salivary gland nuclear
865 markers CrebA (A-C and F) and Sage (D and E). Salivary glands overexpressing Tmem-GFP
866 (control, A), Jbug-RC (B), Jbug-RC-GFP (C), Jbug-RI (D), Jbug-RL (E) and Jbug-RF (F, G) are
867 shown. Note that Jbug mainly localizes to the cytoplasm and only shows weak apical signals in
868 stage 16 salivary glands (red arrow in A; compare to Figure 4E). Jbug-RC (B) and Jbug-RC-GFP
869 (C) localize both to salivary gland nuclei and the cytoplasm when overexpressed. Jbug
870 overexpression causes an expanded and irregular salivary gland lumen (B-G). Irregular salivary
871 gland lumen is worsened when stronger UAS lines are used (compare B and C; also compare F
872 and G). Compared to subapical Crb signals along AJs in control salivary gland cells (inset in A;
873 yellow arrows), Crb signals are dispersed along the entire apical domain in Jbug-overexpressing
874 salivary glands (insets in B-G). (H) Quantification of the irregular apical membrane morphology in
875 salivary glands overexpressing different Jbug isoforms. Strong UAS lines shown in B and G were
876 used to overexpress Jbug-RC and Jbug-RF. For mild irregularity, salivary glands with the uneven
877 apical domain were counted. For severe irregularity, salivary glands with bulging and constriction
878 phenotypes were counted.
879

Figure 7

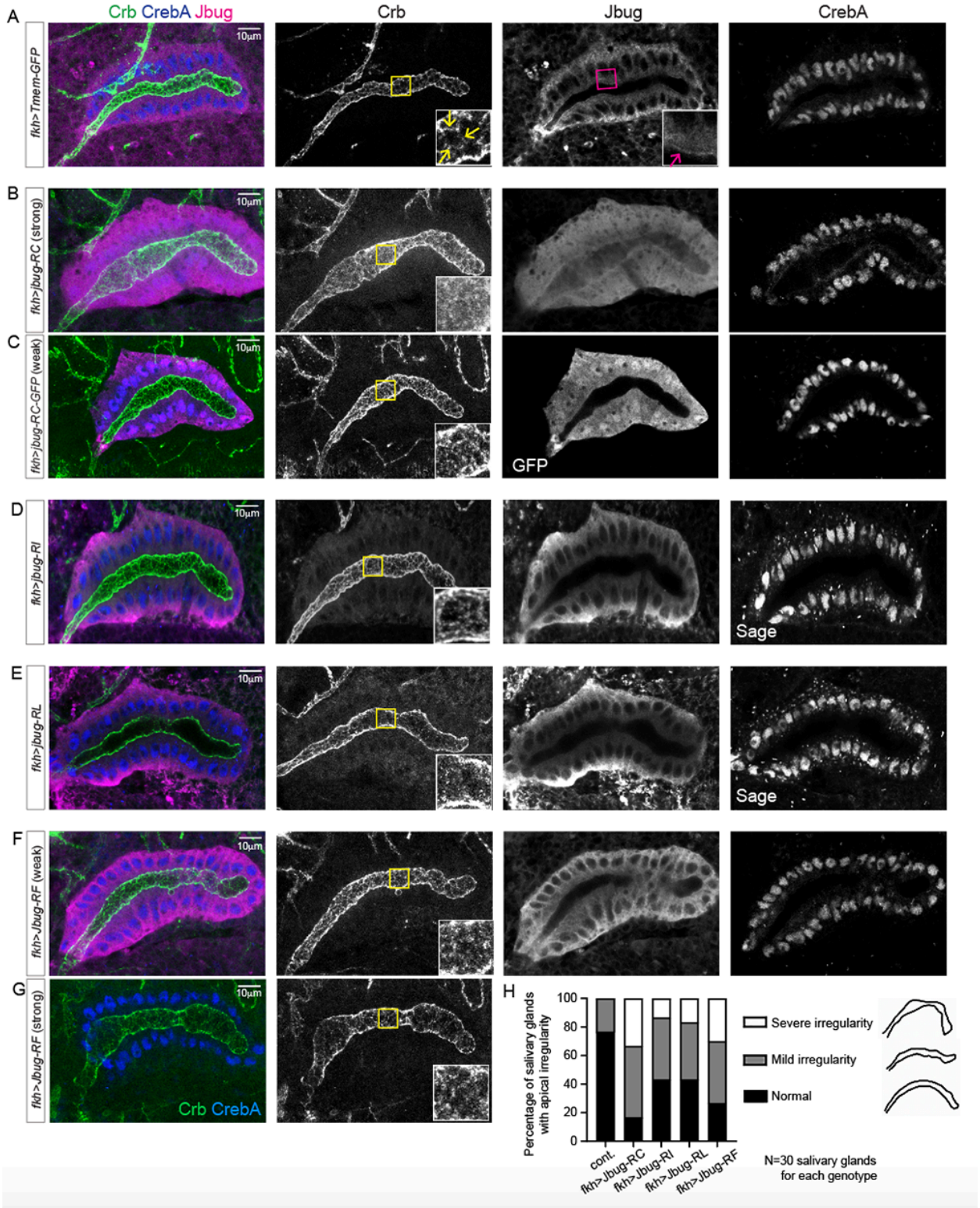

880

881

882 **Figure 8. Jbug is required for proper Crb levels in epithelial cells during embryogenesis.**
883 (A-H) Confocal images of stage 14/15 embryos of control (*da-Gal4/+*; A and E), zygotic (*da>jbug*
884 *RNAi*; B and F), maternal (*matα>jbug RNAi*; C and G), and both maternal and zygotic knockdown
885 of *jbug* (*matα, da>jbug RNAi*; D and H). Anterior is to the left. Ventral (A, D, E), dorsal (F) and
886 lateral (B, C, G and H) views are shown. (A-D) Embryos stained for E-Cad (magenta). (E-H)
887 Embryos stained for Crb (green) and Sage (a SG marker; magenta). (E'-H''') Higher magnification
888 of the boxed regions in E-H. Crb (green) and Jbug (magenta) are shown. Compared to strong
889 apical surface Jbug signals in epidermal cells in control (E'') and embryos knocked down for *jbug*
890 only zygotically (F'') or maternally (G''), Jbug signals are absent in the apical surface in many
891 epidermal cells in *jbug* M/Z knockdown embryos (yellow arrowheads in H' and H''). In those cells,
892 Crb is also absent (yellow arrows in H'''). Compare to neighboring cells with significant apical
893 surface Jbug signals (cyan arrowheads in H' and H'') and relatively normal Crb localization (cyan
894 arrows in H'''). Asterisks, residual or nonspecific Jbug signals. (I-M) Confocal images of stage 14
895 salivary glands stained for Crb (green) and Jbug (magenta). White dotted lines, salivary gland
896 boundaries. Control (*fkh-Gal4/+*; I), zygotic (*fkh>jbug RNAi*; J), maternal (*matα>jbug RNAi*; K),
897 and both maternal and zygotic knockdown of *jbug* (*matα, fkh>jbug RNAi*; two representative
898 images are shown in L and M). (I'-M'') Jbug (I'-M') and Crb (I''-M'') only. Jbug signals are reduced
899 in *jbug* knockdown (cyan arrowheads in J'-M'), with a more significant reduction in maternal (K')
900 and maternal/zygotic knockdown (K'-M'). (I'''-M''') Higher magnification of the boxed regions in I''-
901 M''. Maternal and maternal/zygotic knockdown of *jbug* results in gaps (yellow arrowheads in K'''
902 and M''') or mislocalized Crb signals to the apical surface (red arrowheads in L''').
903

Figure 8

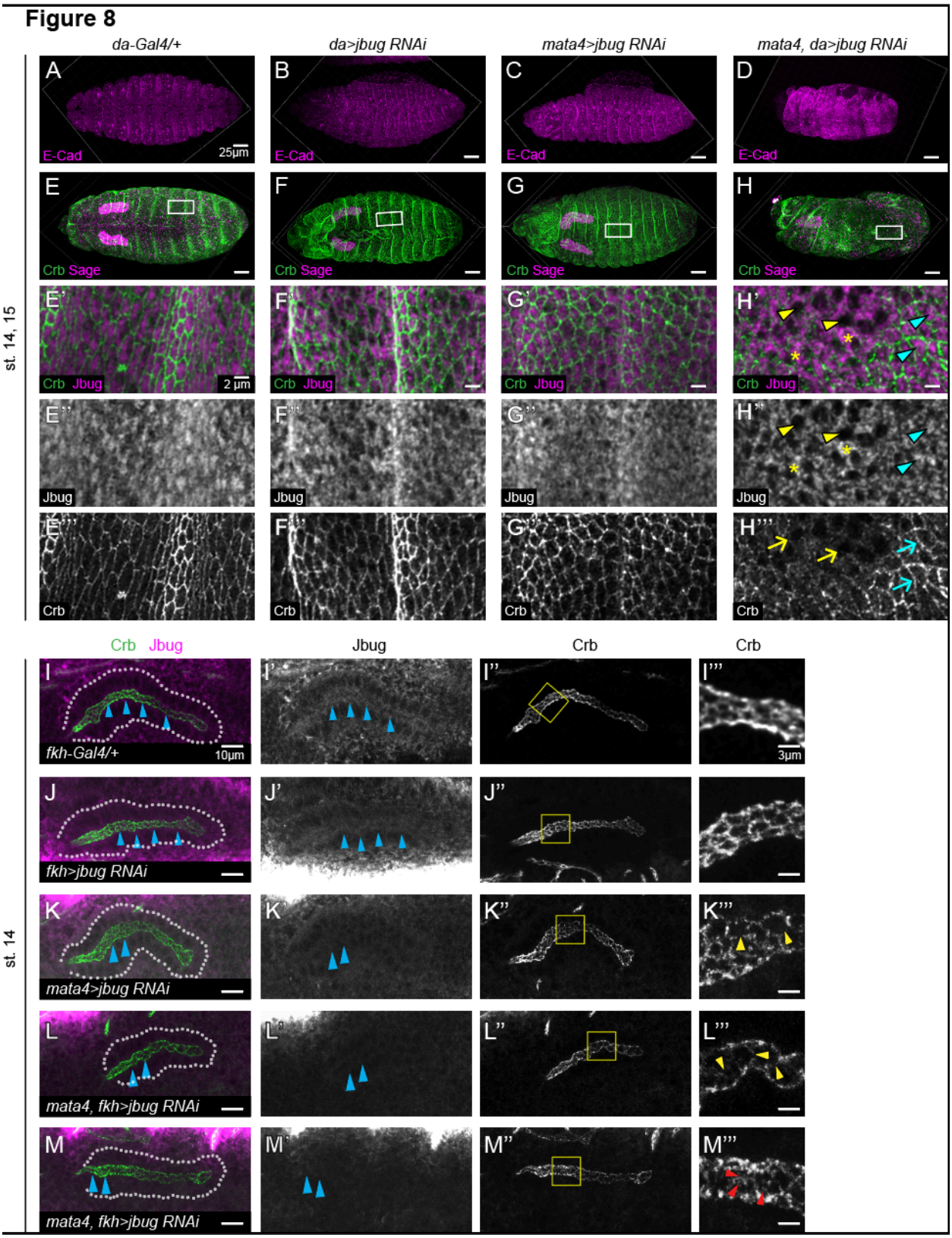
da-Gal4/+
da>jbug RNAi
mata4>jbug RNAi
mata4, da>jbug RNAi
st. 14, 15
A
B
C
D
E-Cad
25µm
E
F
G
H
Crb Sage
E'
F'
G'
H'
Crb Jbug
2 µm
E''
F''
G''
H''
Jbug
E'''
F'''
G'''
H'''
Crb
Crb Jbug
Jbug
Crb
Crb
st. 14
I
I'
I''
I'''
fkh-Gal4/+
10µm
3µm
J
J'
J''
fkh>jbug RNAi
K
K'
K''
K'''
mata4>jbug RNAi
L
L'
L''
L'''
mata4, fkh>jbug RNAi
M
M'
M''
M'''
mata4, fkh>jbug RNAi

904

905 **Figure 9. Isoform-specific roles and features of Jbug.**

906

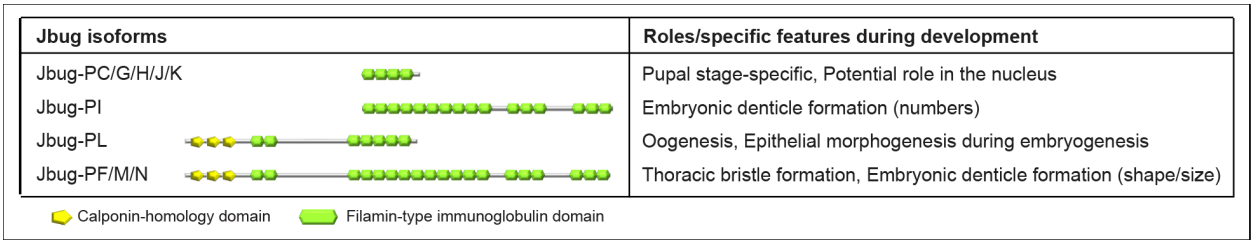

907 **Supplemental Figure 1. In situ hybridization.** In situ hybridization of wild-type embryos using
908 probes specific for different *jbug* splice forms as shown in Figure 1A. CL, clypeolabrum. SG,
909 salivary gland. tp, tracheal pits. PS, posterior spiracles.
910

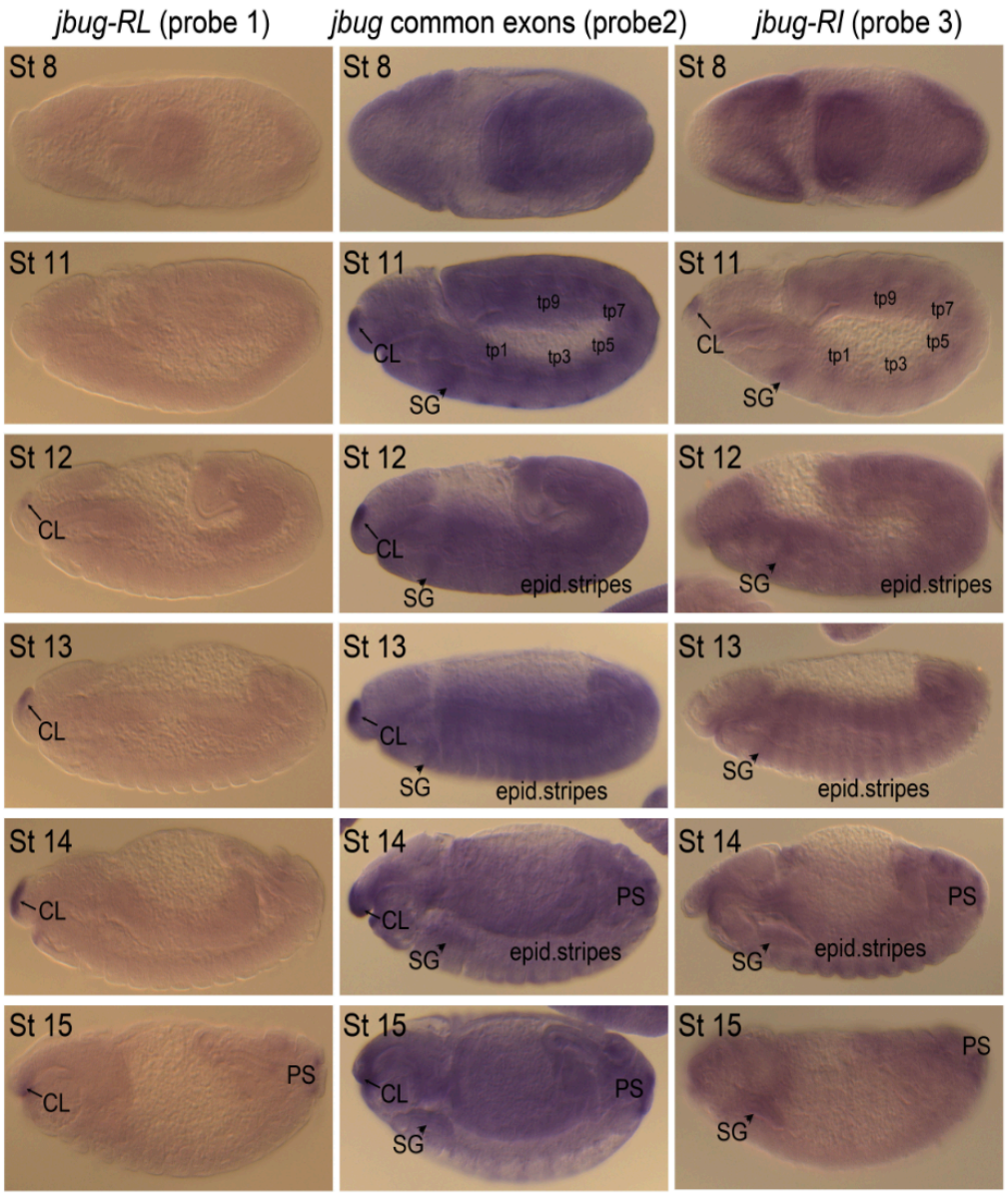

911 **Supplemental Figure 2. Reverse transcriptase-PCR (RT-PCR) reveals a loss of *jbug* mRNA**
912 **in *jbug*^{20} null mutants.** (A) Genomic structures for the jbug locus. Blue and red arrows represent
913 primers used for RT-PCR. (B and C) RT-PCR using cDNAs made from wild-type (OR) and *jbug*^{20}
914 homozygous embryos. Whereas RT-PCR using wild-type cDNA produces a PCR product of
915 expected sizes (left lanes in B and C), no bands are detected in *jbug*^{20} (right lanes in B and C).

916

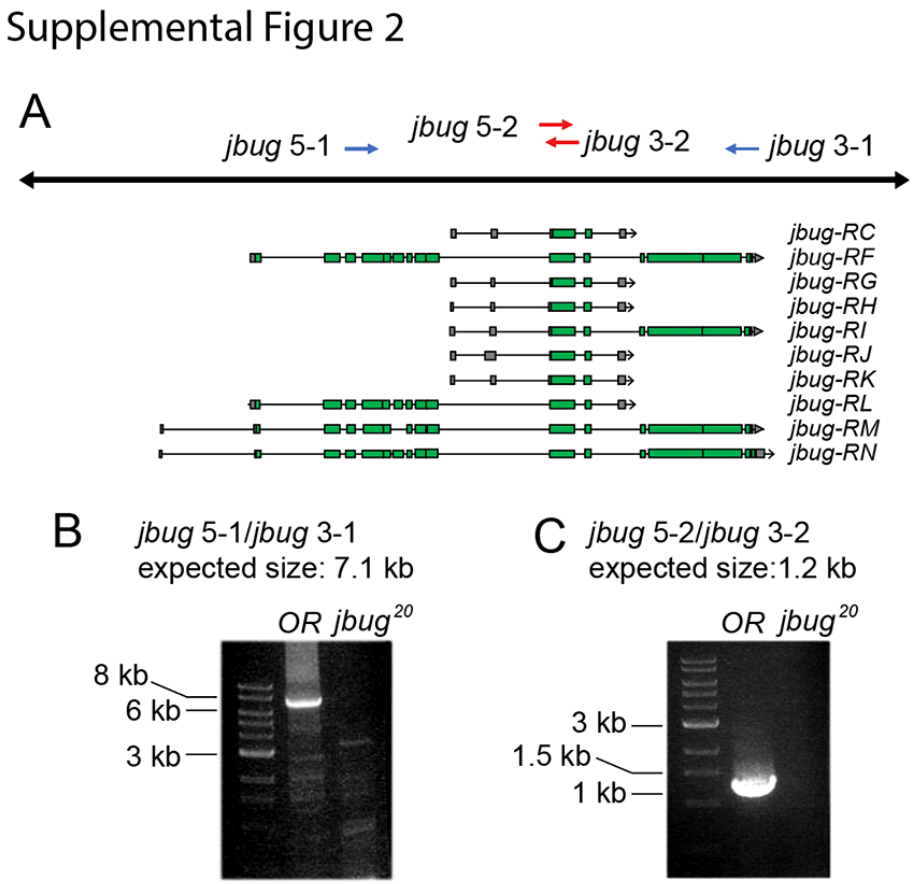

Supplemental Figure 3. Mutations in *jbug* cause mild planar cell polarity defects in adult wing hair orientation. (A-C) Adult wings. Compared to the largely distal orientation of wing hairs in the wild-type wing (A), wings in *jbug*^{30} mutants (B) show mild swirling patterns of wing hairs. (C) *jbug*^{30}*/Exel6079* flies do not show defects in the wing hair orientation. White boxed regions are shown in higher magnification in the bottom. (D, E) Wild-type (D) and *jbug*^{30} mutant (E) pupal wings (32 hours APF) stained for phalloidin. Prehair formation is delayed in the pupal wing in *jbug*^{30}. (F, G) Adult ommatidia of wild type (F) and *jbug*^{30} (G) near the dorsal/ventral boundary, the equator. Schematic drawings are shown in the panels below the actual images. Green and magenta shapes indicate the orientation of ommatidia normally found in the dorsal and ventral hemisphere of the eye, respectively. *jbug*^{30} flies do not show planar cell polarity defects in the orientation of ommatidia.

Supplemental Figure 3

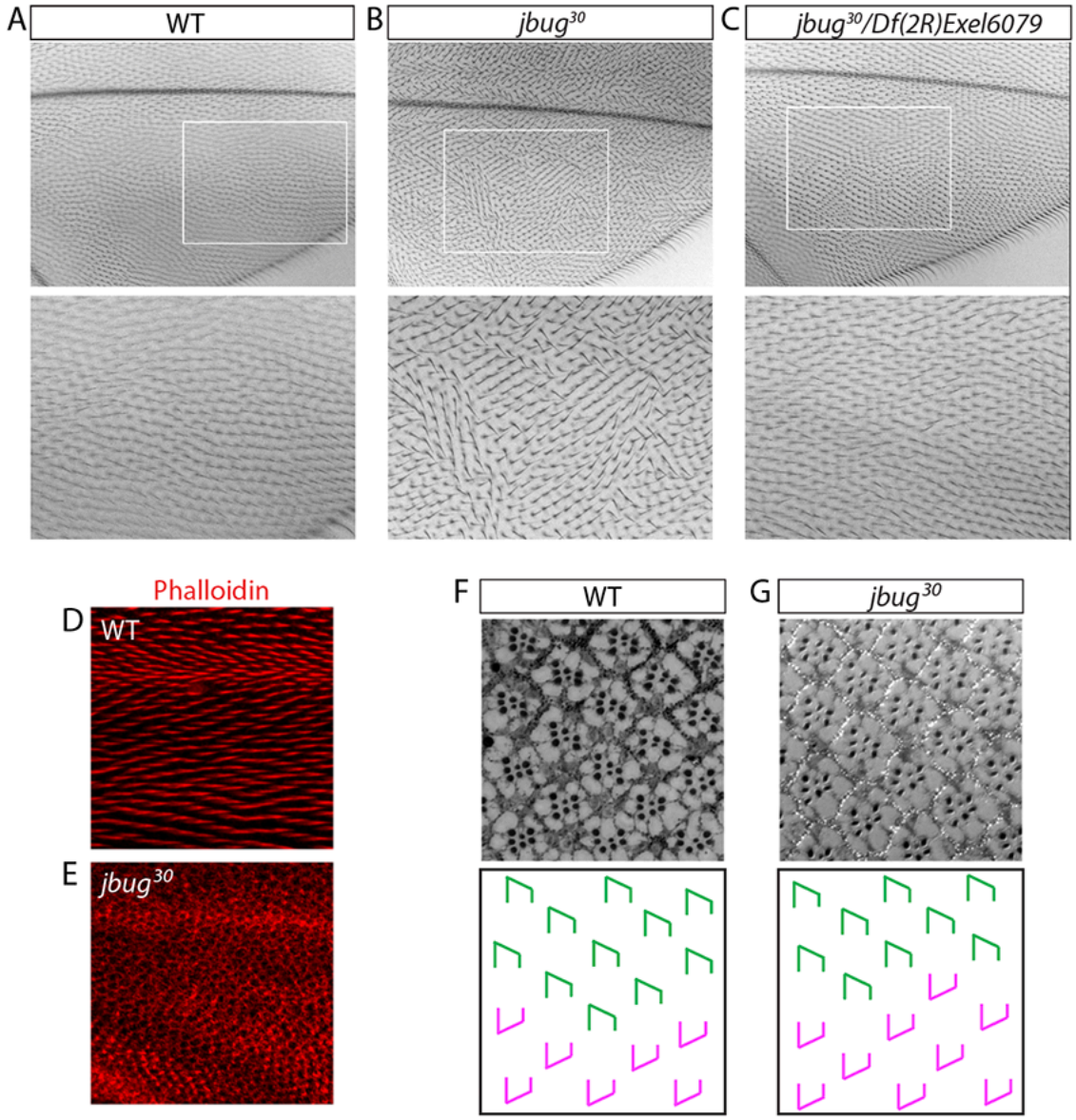

929
930

Supplemental Figure 4. Jbug regulates the formation of denticle precursors in the ventral epidermis of the embryo. (A) Percentage of cells that have different numbers of denticles in rows C2-C5. (B) Quantification of the average number of denticles per cell in C2-C5. Student's t-test with Welch's correction is used for statistics calculation. The same four cells as shown in Figure 5K were chosen for quantification for each genotype.

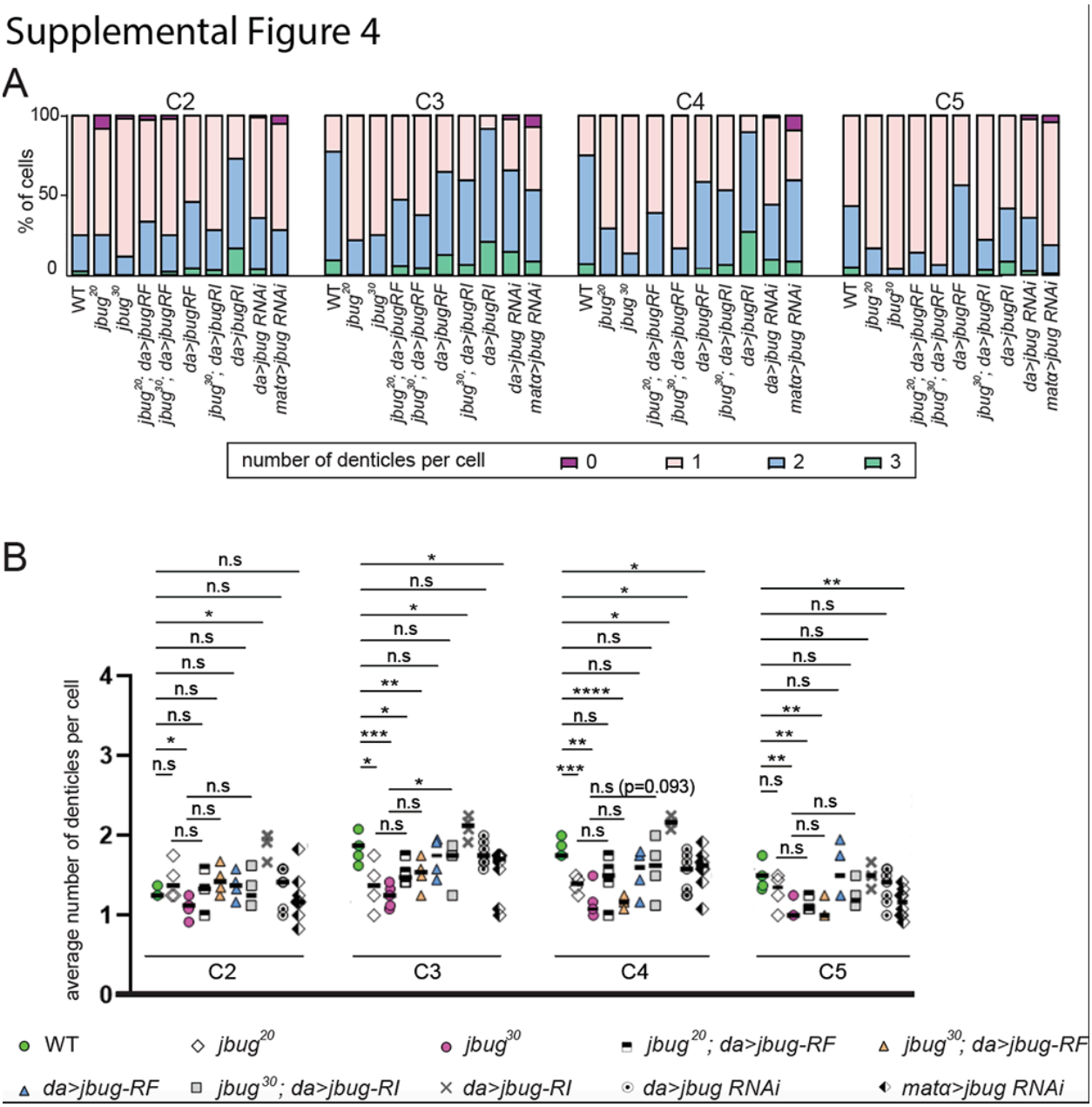

937 **Supplemental Figure 5. Epithelial polarity markers and F-actin and are not affected in**
938 **salivary glands in *jbug* mutants.** (A-I) Confocal images of stage 16 salivary glands. (A-C) Wild-
939 type (A), *jbug*^{20} (B) and *jbug*^{30} (C) salivary glands stained for Crb (green) and E-Cad (magenta).
940 (D-F) Wild-type (E), *jbug*^{20} (F) and *jbug*^{30} (G) salivary glands stained for phalloidin (green) and
941 Dlg (magenta). (G-I) Wild-type (G), *jbug*^{20} (H) and *jbug*^{30} (I) salivary glands stained for α-Spec.
942 Insets, higher magnification of the boxed region.
943

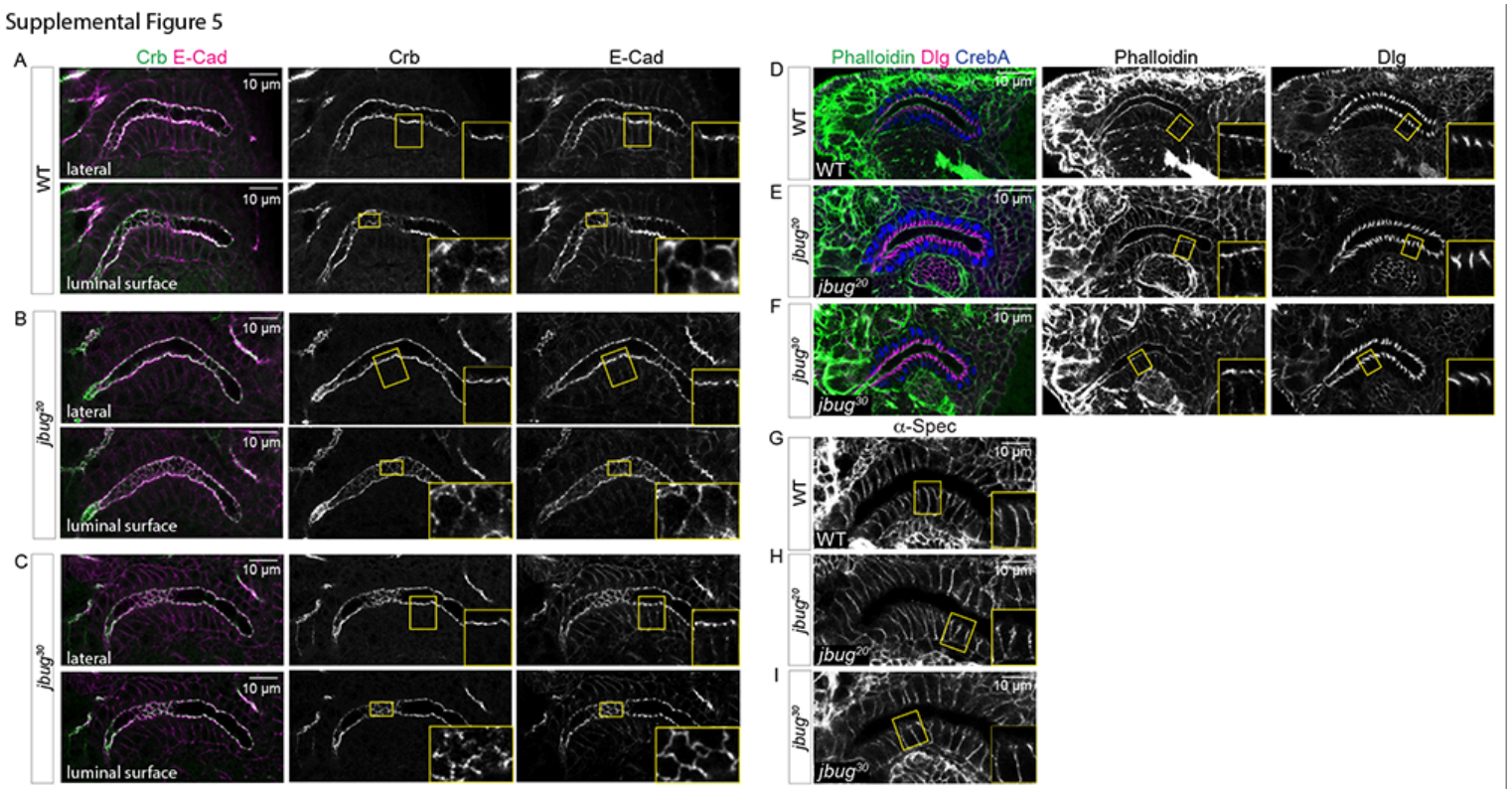

944 **Supplemental Figure 6. F-actin, epithelial polarity markers and junction markers are not**
945 **significantly altered in salivary glands overexpressing different Jbug isoforms.** (A-J)
946 Confocal images of stage 16 control (*fkh-Gal4/+*, A and F) and salivary glands overexpressing
947 Jbug-RC (B and G), Jbug-RI (C and H), Jbug-RL (D and I) and Jbug-RF (E and J). (A-E) Salivary
948 gland stained for phalloidin (green), α-Spec (magenta) and a salivary gland nuclear marker CrebA
949 (blue). (F-J) Salivary glands stained for Nrx-IV (green) and E-Cad (magenta). Insets, higher
950 magnification of the boxed region.
951

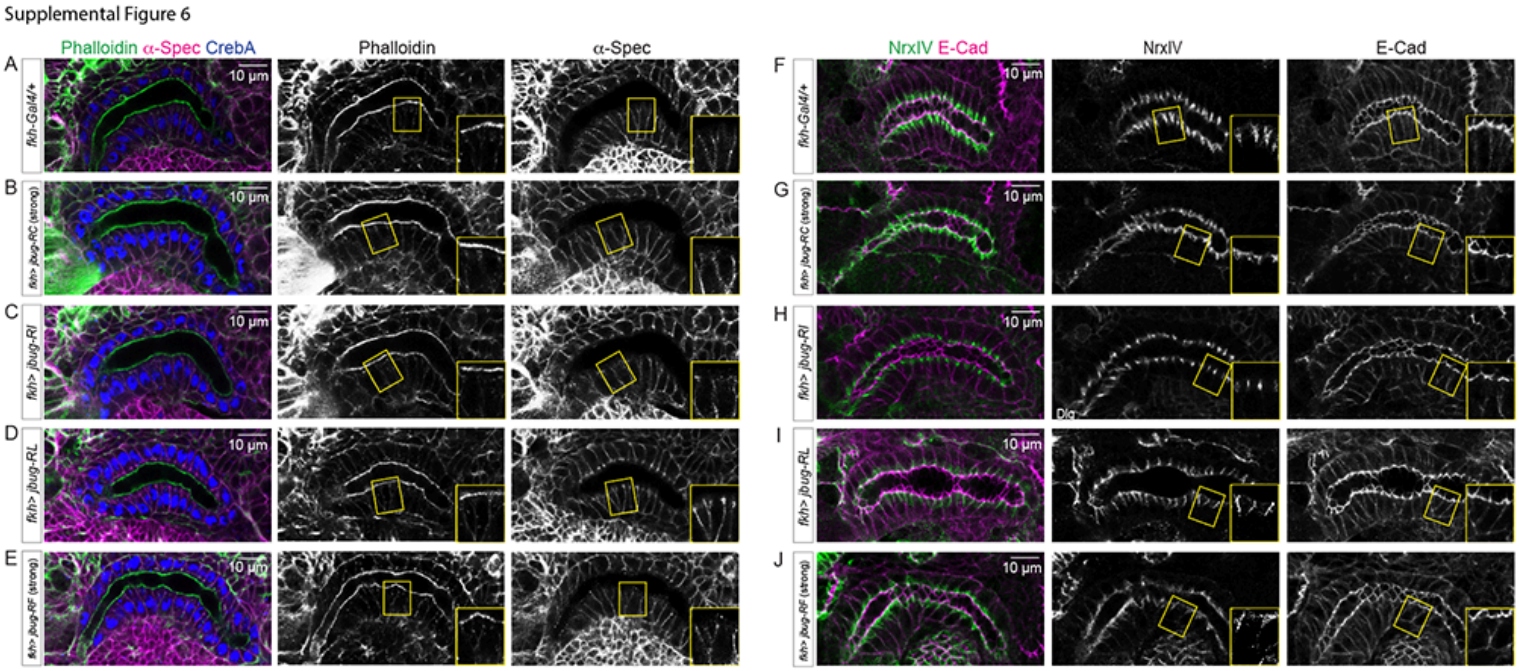

952 **Supplemental Figure 7.** (A-D) Confocal images of stage 11 embryos stained for Crb (green),
953 and Sage (blue). Control (*fkh-Gal4/+*; A), zygotic (*fkh>jbug RNAi*; B), maternal (*matα>jbug RNAi*;
954 C), and both maternal and zygotic knockdown of *jbug* (*matα, fkh>jbug RNAi*; D). (A'-D''') Higher
955 magnification of the salivary glands in A-D. Crb (green), Jbug (magenta) and Sage (blue) signals
956 are shown. (A''-D''') Crb (A''-D'') and Jbug (A'''-D''') only. Jbug signals are slightly reduced in *jbug*
957 knockdown, with a more significant reduction in maternal (C''') and maternal/zygotic knockdown
958 (D'''). (A'''-D'''') Higher magnification of the boxed region in A''-D''. Maternal/zygotic knockdown
959 of *jbug* results in gaps (yellow arrowheads) and mislocalized Crb signals to the apical surface (red
960 arrowheads).

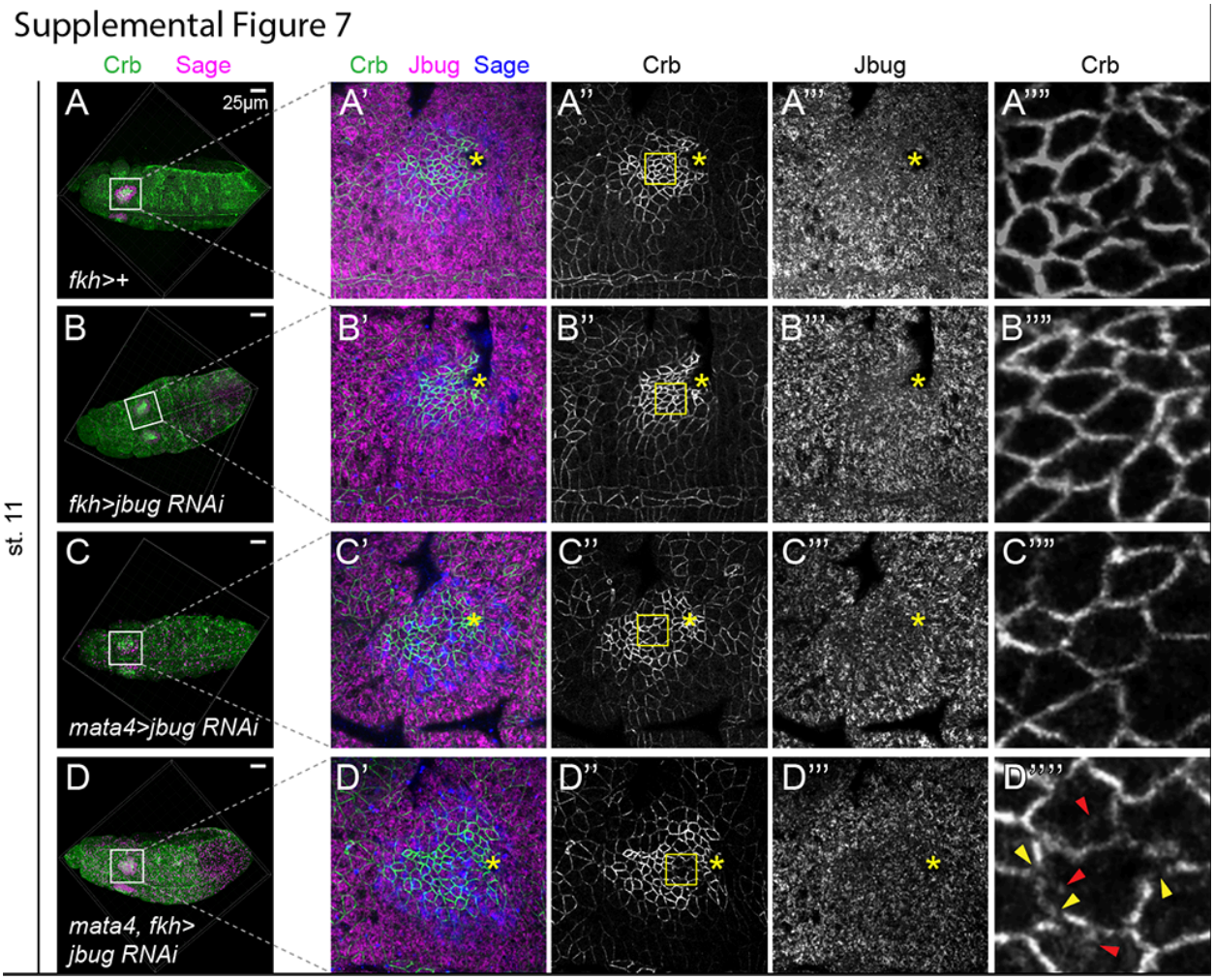

961

Acknowledgments

We thank the members of the Chung and the Andrew laboratories for their comments and suggestions. We thank M. Mlodzik and the Bloomington stock center for fly stocks and the Developmental Studies Hybridoma Bank for antibodies. We thank Flybase for the gene information. This work is supported by start-up fund from Louisiana State University to S.C. and NIH R01 DE013899 to D.J.A.

969 **References**

970 Adler P. N., 2012 The frizzled/stan pathway and planar cell polarity in the Drosophila wing. Curr.
971 Top. Dev. Biol. 101: 1–31. https://doi.org/10.1016/b978-0-12-394592-1.00001-6
972 Baumgartner S., J. T. Littleton, K. Broadie, M. A. Bhat, R. Harbecke, *et al.*, 1996 A Drosophila
973 neurexin is required for septate junction and blood-nerve barrier formation and function.
974 Cell 87: 1059–1068. https://doi.org/10.1016/S0092-8674(00)81800-0
975 Bedolla R. G., Y. Wang, A. Asuncion, K. Chamie, S. Siddiqui, *et al.*, 2009 Nuclear versus
976 cytoplasmic localization of filamin a in prostate cancer: Immunohistochemical correlation
977 with metastases. Clin. Cancer Res. 15: 788–796. https://doi.org/10.1158/1078-0432.CCR-
978 08-1402
979 Bejsovec A., 2013 Wingless/Wnt signaling in Drosophila: The pattern and the pathway. Mol.
980 Reprod. Dev. 80: 882–894. https://doi.org/10.1002/mrd.22228
981 Bellanger J. M., C. Astier, C. Sardet, Y. Ohta, T. P. Stossel, *et al.*, 2000 The Rac1- and RhoG-
982 specific GEF domain of trio targets filamin to remodel cytoskeletal actin. Nat. Cell Biol. 2:
983 888–892. https://doi.org/10.1038/35046533
984 Blanchoin L., K. J. Amann, H. N. Higgs, J. Marchand, D. A. Kaiser, *et al.*, 2000 Direct
985 observation of dendritic actin ®lamentnetworksnucleatedbyArp2/3 complex and
986 WASP/Scar proteins. Nature 404: 1007–1011. https://doi.org/10.1038/35010008
987 Browne K. A., R. W. Johnstone, D. A. Jans, and J. A. Trapani, 2000 Filamin (280-kDa actin-
988 binding protein) is a caspase substrate and is also cleaved directly by the cytotoxic T
989 lymphocyte protease granzyme B during apoptosis. J. Biol. Chem. 275: 39262–39266.
990 https://doi.org/10.1074/jbc.C000622200
991 Chung S. Y., C. Chavez, and D. J. Andrew, 2011 Trachealess (Trh) regulates all tracheal genes
992 during Drosophila embryogenesis. Dev. Biol. 360: 160–172.
993 https://doi.org/10.1016/j.ydbio.2011.09.014
994 Chung S., and D. J. Andrew, 2014 Cadherin 99C regulates apical expansion and cell
995 rearrangement during epithelial tube elongation. Development 141: 1950–60.
996 https://doi.org/10.1242/dev.104166
997 Cunningham C. C., J. B. Gorlin, D. J. Kwiatkowski, J. H. Hartwig, A. Janmey, *et al.*, 1992 Actin-
998 Binding Protein Requirement for Cortical Stability and Efficient Locomotion Published by :
999 American Association for the Advancement of Science Stable URL :
1000 http://www.jstor.org/stable/2876160. Science (80-.). 255: 325–327.
1001 https://doi.org/10.1126/science.1549777
1002 Dilks S. A., and S. DiNardo, 2010 Non-cell-autonomous control of denticle diversity in the

1003 Drosophila embryo. Development 137: 1395–1404. https://doi.org/10.1242/dev.045450
1004 Flier A. Van der, and A. Sonnenberg, 2001 Structural and functional aspects of filamins.
1005 Biochim. Biophys. Acta - Mol. Cell Res. 1538: 99–117. https://doi.org/10.1016/S0167-
1006 4889(01)00072-6
1007 Fox R. M., A. Vaishnavi, R. Maruyama, and D. J. Andrew, 2013 Organ-specific gene
1008 expression: The bHLH protein Sage provides tissue specificity to Drosophila FoxA. Dev.
1009 140: 2160–2171. https://doi.org/10.1242/dev.092924
1010 Frank D. J., R. Hopmann, M. Lenartowska, and K. G. Miller, 2006 Capping Protein and the
1011 Arp2/3 Complex Regulate Nonbundle Actin Filament Assembly to Indirectly Control Actin
1012 Bundle Positioning during Drosophila melanogaster Bristle Development. Mol. Biol. Cell 17:
1013 3930–3939. https://doi.org/10.1091/mbc.E06-06-0500
1014 Gao J. L., Y. J. Fan, X. Y. Wang, Y. Zhang, J. Pu, *et al.*, 2015 A conserved intronic U1 snRNP-
1015 binding sequence promotes trans-splicing in Drosophila. Genes Dev. 29: 760–771.
1016 https://doi.org/10.1101/gad.258863.115
1017 Gay O., B. Gilquin, F. Nakamura, Z. A. Jenkins, R. McCartney, *et al.*, 2011 RefilinB (FAM101B)
1018 targets FilaminA to organize perinuclear actin networks and regulates nuclear shape. Proc.
1019 Natl. Acad. Sci. U. S. A. 108: 11464–11469. https://doi.org/10.1073/pnas.1104211108
1020 Gehler S., M. Baldassarre, Y. Lad, J. L. Leight, M. A. Wozniak, *et al.*, 2009 Filamin A–β1
1021 Integrin Complex Tunes Epithelial Cell Response to Matrix Tension. Mol. Biol. Cell 20:
1022 3224–3238. https://doi.org/10.1091/mbc.E08
1023 Gong W. J., and K. G. Golic, 2003 Ends-out, or replacement, gene targeting in Drosophila.
1024 Proc. Natl. Acad. Sci. U. S. A. 100: 2556–2561. https://doi.org/10.1073/pnas.0535280100
1025 Gorlin J. B., R. Yamin, S. Egan, M. Stewart, T. P. Stossel, *et al.*, 1990 Human endothelial actin-
1026 binding protein (ABP-280, nonmuscle filamin): A molecular leaf spring. J. Cell Biol. 111:
1027 1089–1105. https://doi.org/10.1083/jcb.111.3.1089
1028 Häcker U., and N. Perrimon, 1998 DRhoGEF2 encodes a member of the Dbl family of
1029 oncogenes and controls cell shape changes during gastrulation in Drosophila. Genes Dev.
1030 12: 274–284. https://doi.org/10.1101/gad.12.2.274
1031 Henderson K. D., and D. J. Andrew, 2000 Regulation and function of Scr, exd, and hth in the
1032 Drosophila salivary gland. Dev. Biol. 217: 362–374. https://doi.org/10.1006/dbio.1999.9560
1033 Horiuchi T., and T. Aigaki, 2006 Alternative trans-splicing: a novel mode of pre-mRNA
1034 processing. Biol. Cell 98: 135–140. https://doi.org/10.1042/bc20050002
1035 Hudson A. M., and L. Cooley, 2002 A subset of dynamic actin rearrangements in Drosophila
1036 requires the Arp2/3 complex. J. Cell Biol. 156: 677–687.

1037 https://doi.org/10.1083/jcb.200109065
1038 Huelsmann S., N. Rintanen, R. Sethi, N. H. Brown, and J. Ylänne, 2016 Evidence for the
1039 mechanosensor function of filamin in tissue development. Sci. Rep. 6: 2–9.
1040 https://doi.org/10.1038/srep32798
1041 Jeon Y. J., J. S. Choi, J. Y. Lee, K. R. Yu, S. H. Ka, *et al.*, 2008 Filamin B Serves as a Molecular
1042 Scaffold for Type I Interferon-induced c-Jun NH2-terminal Kinase Signaling Pathway. Mol.
1043 Biol. Cell 19: 5116–5130. https://doi.org/10.1091/mbc.e08-06-0576
1044 King T. D., J. E. Johnson, and J. R. Bateman, 2019 Position Effects In fl uence Transvection in.
1045 213: 1289–1299. https://doi.org/https://doi.org/10.1534/genetics.119.302583
1046 Krueger D., T. Quinkler, S. A. Mortensen, C. Sachse, and S. de Renzis, 2019 Cross-linker–
1047 mediated regulation of actin network organization controls tissue morphogenesis. J. Cell
1048 Biol. 218: 2743–2761. https://doi.org/10.1083/JCB.201811127
1049 Külshammer E., and M. Uhlirova, 2013 The actin cross-linker filamin/cheerio mediates tumor
1050 malignancy downstream of JNK signaling. J. Cell Sci. 126: 927–938.
1051 https://doi.org/10.1242/jcs.114462
1052 Lasda E. L., and T. Blumenthal, 2011 Trans-splicing. Wiley Interdiscip. Rev. RNA 2: 417–434.
1053 https://doi.org/10.1002/wrna.71
1054 Lee G. Y., and T. L. Schwarz, 2016 Filamin, a synaptic organizer in Drosophila, determines
1055 glutamate receptor composition and membrane growth. Elife 5: 1–29.
1056 https://doi.org/10.7554/eLife.19991
1057 Lehmann R., and D. Tautz, 1994 In Situ Hybridization to RNA. Methods Cell Biol. 44: 575–598.
1058 https://doi.org/doi: 10.1016/s0091-679x(08)60933-4
1059 Li M., M. Serr, K. Edwards, S. Ludmann, D. Yamamoto, *et al.*, 1999 during Drosophila
1060 Oogenesis. Cell 146: 1061–1073.
1061 Loy C. J., K. S. Sim, and E. L. Yong, 2003 Filamin-A fragment localizes to the nucleus to
1062 regulate androgen receptor and coactivator functions. Proc. Natl. Acad. Sci. U. S. A. 100:
1063 4562–4567. https://doi.org/10.1073/pnas.0736237100
1064 Mammoto A., S. Huang, and D. E. Ingber, 2007 Filamin links cell shape and cytoskeletal
1065 structure to Rho regulation by controlling accumulation of p190RhoGAP in lipid rafts. J. Cell
1066 Sci. 120: 456–467. https://doi.org/10.1242/jcs.03353
1067 Manieu C., G. H. Olivares, F. Vega-Macaya, M. Valdivia, and P. Olguín, 2018 Jitterbug/Filamin
1068 and Myosin-II form a complex in tendon cells required to maintain epithelial shape and
1069 polarity during musculoskeletal system development. Mech. Dev. 154: 309–314.
1070 https://doi.org/10.1016/j.mod.2018.09.002

1071 Mongelard F., M. Labrador, E. M. Baxter, T. I. Gerasimova, and V. G. Corces, 2002 Trans-
1072 splicing as a novel mechanism to explain interallelic complementation in Drosophila.
1073 Genetics 160: 1481–1487.
1074 Mullins R. D., J. A. Heuser, and T. D. Pollard, 1998 The interaction of Arp2/3 complex with actin:
1075 Nucleation, high affinity pointed end capping, and formation of branching networks of
1076 filaments. Proc. Natl. Acad. Sci. U. S. A. 95: 6181–6186.
1077 https://doi.org/10.1073/pnas.95.11.6181
1078 Nakamura F., O. Heikkinen, O. T. Pentikäinen, T. M. Osborn, K. E. Kasza, *et al.*, 2009
1079 Molecular basis of filamin A-FilGAP interaction and its impairment in congenital disorders
1080 associated with Filamin A mutations. PLoS One 4.
1081 https://doi.org/10.1371/journal.pone.0004928
1082 Nakamura F., T. P. Stossel, and J. H. Hartwig, 2011 The filamins: Organizers of cell structure
1083 and function. Cell Adh. Migr. 5: 160–169. https://doi.org/10.4161/cam.5.2.14401
1084 Niederman R., P. C. Amrein, and J. Hartwig, 1983 Three-dimensional structure of actin
1085 filaments and of an actin gel made with actin-binding protein. J. Cell Biol. 96: 1400–1413.
1086 https://doi.org/10.1083/jcb.96.5.1400
1087 Ohsako T., T. Horiuchi, T. Matsuo, S. Komaya, and T. Aigaki, 2003 Drosophila lola encodes a
1088 family of BTB-transcription regulators with highly variable C-terminal domains containing
1089 zinc finger motifs. Gene 311: 59–69. https://doi.org/10.1016/S0378-1119(03)00554-7
1090 Ohta Y., and J. H. Hartwig, 1996 Phosphorylation of actin-binding protein 280 by growth factors
1091 is mediated by p90 ribosomal protein S6 kinase. J. Biol. Chem. 271: 11858–11864.
1092 https://doi.org/10.1074/jbc.271.20.11858
1093 Ohta Y., N. Suzuki, S. Nakamura, J. H. Hartwig, and T. P. Stossel, 1999 The small GTPase
1094 RalA targets filamin to induce filopodia. Proc. Natl. Acad. Sci. U. S. A. 96: 2122–2128.
1095 https://doi.org/10.1073/pnas.96.5.2122
1096 Ohta Y., J. H. Hartwig, and T. P. Stossel, 2006 FilGAP, a Rho- and ROCK-regulated GAP for
1097 Rac binds filamin A to control actin remodelling. Nat. Cell Biol. 8: 803–814.
1098 https://doi.org/10.1038/ncb1437
1099 Olguín P., A. Glavic, and M. Mlodzik, 2011 Intertissue mechanical stress affects Frizzled-
1100 mediated planar cell polarity in the Drosophila notum epidermis. Curr. Biol. 21: 236–42.
1101 https://doi.org/10.1016/j.cub.2011.01.001
1102 Oliva C., C. Molina-Fernandez, M. Maureira, N. Candia, E. L??pez, *et al.*, 2015 Hindsight
1103 regulates photoreceptor axon targeting through transcriptional control of jitterbug/Filamin
1104 and multiple genes involved in axon guidance in Drosophila. Dev. Neurobiol. 75: 1018–

1032. https://doi.org/10.1002/dneu.22271

Pi M., R. F. Spurney, Q. Tu, T. Hinson, and L. D. Quarles, 2002 Calcium-sensing receptor activation of Rho involves filamin and rho-guanine nucleotide exchange factor. Endocrinology 143: 3830–3838. https://doi.org/10.1210/en.2002-220240

Razinia Z., T. Mäkelä, J. Ylänne, and D. a Calderwood, 2012 Filamins in mechanosensing and signaling. Annu. Rev. Biophys. 41: 227–46. https://doi.org/10.1146/annurev-biophys-050511-102252

Rorth Pe., 1996 A modular misexpression screen in Drosophila detecting tissue-specific phenotypes. Proc. Natl. Acad. Sci. 93: 12418–12422.

Sasaki E., A. T. Byrne, E. Phelan, D. W. Cox, and W. Reardon, 2019 A review of filamin A mutations and associated interstitial lung disease. Eur. J. Pediatr. 178: 121–129. https://doi.org/10.1007/s00431-018-3301-0

Savoy R. M., and P. M. Ghosh, 2013 The dual role of filamin A in cancer: Can't live with (too much of) it, can't live without it. Endocr. Relat. Cancer 20: 341–356. https://doi.org/10.1530/ERC-13-0364

Shao Q. Q., T. P. Zhang, W. J. Zhao, Z. W. Liu, L. You, *et al.*, 2016 Filamin A: Insights into its Exact Role in Cancers. Pathol. Oncol. Res. 22: 245–252. https://doi.org/10.1007/s12253-015-9980-1

Sokol N. S., and L. Cooley, 1999 Drosophila Filamin encoded by the cheerio locus is a component of ovarian ring canals. Curr. Biol. 9: 1221–1230. https://doi.org/10.1016/S0960-9822(99)80502-8

Sokol N. S., and L. Cooley, 2003 Drosophila filamin is required for follicle cell motility during oogenesis. Dev. Biol. 260: 260–272. https://doi.org/10.1016/S0012-1606(03)00248-3

Song J., and M. A. Tanouye, 2006 Seizure suppression by shakB2, a gap junction mutation in Drosophila. J. Neurophysiol. 95: 627–635. https://doi.org/10.1152/jn.01059.2004

Tepass U., 1996 Crumbs, a component of the apical membrane, is required for zonula adherens formation in primary epithelia of Drosophila. Dev. Biol. 177: 217–225. https://doi.org/10.1006/dbio.1996.0157

Thurmond J., J. L. Goodman, V. B. Strelets, H. Attrill, L. S. Gramates, *et al.*, 2019 FlyBase 2.0: The next generation. Nucleic Acids Res. 47: D759–D765. https://doi.org/10.1093/nar/gky1003

Tikhonov M., M. Utkina, O. Maksimenko, and P. Georgiev, 2018 Conserved sequences in the Drosophila mod(mdg4) intron promote poly(A)-independent transcription termination and trans-splicing. Nucleic Acids Res. 46: 10608–10618. https://doi.org/10.1093/nar/gky716

1139 Tirupula K. C., S. S. Ithychanda, M. L. Mohan, S. V. Naga Prasad, J. Qin, *et al.*, 2015 G protein-
1140 coupled receptors directly bind filamin A with high affinity and promote filamin
1141 phosphorylation. Biochemistry 54: 6673–6683.
1142 https://doi.org/10.1021/acs.biochem.5b00975
1143 Ueda K., Y. Ohta, and H. Hosoya, 2003 The carboxy-terminal pleckstrin homology domain of
1144 ROCK interacts with filamin-A. Biochem. Biophys. Res. Commun. 301: 886–890.
1145 https://doi.org/10.1016/S0006-291X(03)00048-2
1146 Valle-Pérez B. Del, V. G. Martínez, C. Lacasa-Salavert, A. Figueras, S. S. Shapiro, *et al.*, 2010
1147 Filamin B plays a key role in vascular endothelial growth factor-induced endothelial cell
1148 motility through its interaction with Rac-1 and Vav-2. J. Biol. Chem. 285: 10748–10760.
1149 https://doi.org/10.1074/jbc.M109.062984
1150 Wang Y., J. I. Kreisberg, R. G. Bedolla, M. Mikhailova, R. W. Devere White, *et al.*, 2007 A 90
1151 kDa fragment of filamin A promotes Casodex-induced growth inhibition in Casodex-
1152 resistant androgen receptor positive C4-2 prostate cancer cells. Oncogene 26: 6061–6070.
1153 https://doi.org/10.1038/sj.onc.1210435
1154 Wang Q., W. Zheng, Z. Wang, J. W. Yang, S. Hussein, *et al.*, 2015 Filamin-A increases the
1155 stability and plasma membrane expression of polycystin-2. PLoS One 10: 1–19.
1156 https://doi.org/10.1371/journal.pone.0123018
1157 Wodarz A., U. Hinz, M. Engelbert, and E. Knust, 1995 Expression of crumbs confers apical
1158 character on plasma membrane domains of ectodermal epithelia of drosophila. Cell 82:
1159 67–76. https://doi.org/10.1016/0092-8674(95)90053-5
1160 Wolosewick J. J., and J. Condeelis, 1986 Fine structure of gels prepared from an actin-binding
1161 protein and actin: Comparison to cytoplasmic extracts and cortical cytoplasm in amoeboid
1162 cells of Dictyostelium discoideum. J. Cell. Biochem. 30: 227–243.
1163 https://doi.org/10.1002/jcb.240300305
1164 Yue J., S. Huhn, and Z. Shen, 2013 Complex roles of filamin-A mediated cytoskeleton network
1165 in cancer progression. Cell Biosci. 3: 1. https://doi.org/10.1186/2045-3701-3-7
1166